ENVIRONMENTAL STUDIES

Exposure to isocyanates predicts atopic dermatitis prevalence and disrupts therapeutic pathways in commensal bacteria

Jordan Zeldin[1], Prem Prashant Chaudhary[1], Jacquelyn Spathies[1], Manoj Yadav[1], Brandon N. D'Souza[1], Mohammadali E. Alishahedani[1], Portia Gough[1], Jobel Matriz[1], Andrew J. Ghio[2], Yue Li[3], Ashleigh A. Sun[1], Lawrence F. Eichenfield[4,5]†, Eric L. Simpson[6]†, Ian A. Myles[1]*

Atopic dermatitis (AD) is a chronic inflammatory skin condition increasing in industrial nations at a pace that suggests environmental drivers. We hypothesize that the dysbiosis associated with AD may signal microbial adaptations to modern pollutants. Having previously modeled the benefits of health-associated *Roseomonas mucosa*, we now show that *R. mucosa* fixes nitrogen in the production of protective glycerolipids and their ceramide by-products. Screening EPA databases against the clinical visit rates identified diisocyanates as the strongest predictor of AD. Diisocyanates disrupted the production of beneficial lipids and therapeutic modeling for isolates of *R. mucosa* as well as commensal *Staphylococcus*. Last, while topical *R. mucosa* failed to meet commercial end points in a placebo-controlled trial, the subgroup who completed the full protocol demonstrated sustained, clinically modest, but statistically significant clinical improvements that differed by study site diisocyanate levels. Therefore, diisocyanates show temporospatial and epidemiological association with AD while also inducing eczematous dysbiosis.

INTRODUCTION

Atopic dermatitis (AD) is a chronic inflammatory skin condition associated with marked psychosocial burdens and allergic sequelae (*1*). The prominent AD paradigm is that the disease has a multifactorial pathology, but with frequent reference to genetic predispositions causing defects in barrier and/or inflammatory pathways. However, the stark post-industrialization increase in AD prevalence (*2*) strongly suggests that environmental factors must play a substantive role. An environmentally focused hypothesis for AD pathogenesis would be consistent not only with the modern rise in AD but also with other epidemiological observations including the protective effects of siblings (*3*, *4*) and early-life migration (*5*, *6*), and the urban-rural divide within genetically similar populations (*7*).

Although the strongest evidence related to the protective effects of cutaneous coagulase-negative Staphylococcus (CoNS), recent work has identified other commensals in the skin and gut as targetable contributors to AD pathogenesis (*8*–*12*). Here, we propose that metabolic differences between health- and disease-associated microbes may represent adaptations to a polluted environment that confer survival benefit to the commensal organism at the expense of symbiotic metabolic pathways. Disease-differentiating microbes, some of which have been shown to govern allergic inflammation in the skin (*13*), could thus serve to screen exposures that are both associated with the disease of interest and influence the distinguishing metabolic pathways in the microbiota.

We previously demonstrated that, while lower in abundance than staphylococcal species, *Roseomonas mucosa* is a skin commensal more frequently found on the skin of health controls than patients with AD (*14*, *15*). Isolates of *R. mucosa* from healthy volunteers (*Rm*HV) directly inhibited the growth of *Staphylococcus aureus* and improved modeled outcomes in mice, while isolates from patients with AD (*Rm*AD) either failed to improve or worsened these modeled outcomes (*14*). Initial open-label clinical results from topical treatment with *Rm*HV demonstrated improvements that lasted beyond active treatment, which were likely due to colonization of patients with the therapeutic strains (*8*). Our mechanistic evaluations demonstrated that the *Rm*HV improved outcomes via lipid mediators, which operate through potentiation of tumor necrosis factor receptor 2 (TNFR2) to induce established pathways of epithelial repair and inhibit the allergic mediators interleukin-13 (IL-13) and thymus and activation-regulated cytokine (TARC) (*8*). We further elucidated a potential direct role for topical skin care products in the development of AD-associated dysbiosis related to both *Rm*HV and commensal isolates of *Staphylococcus* (*16*).

Here, we identify that isolates of *Rm*HV are environmentally sensitive, beneficial commensals that use nitrogen fixation in the production of glycerolipids and their ceramide by-products. We also identify diisocyanates and hydrogen isocyanate (HNCO) as the environmental exposures with the strongest association with AD prevalence and show that they disrupted symbiotic pathways in health-associated strains of both *R. mucosa* and CoNS. Furthermore, increased exposure to (di)isocyanates from factories, catalytic conversion of gasoline, and in-home products coincide with both the historical rise in AD prevalence and published epidemiologic

[1]Epithelial Therapeutics Unit, National Institute of Allergy and Infectious Disease, National Institutes of Health, Bethesda, MD, USA. [2]U.S. Environmental Protection Agency, Chapel Hill, NC, USA. [3]Department of Chemistry and Biochemistry, University of Maryland, College Park, MD, USA. [4]Departments of Dermatology and Pediatrics, University of California San Diego, La Jolla, CA, USA. [5]Rady Children's Hospital, San Diego, CA, USA. [6]Department of Dermatology, Oregon Health and Science University, Portland, OR, USA.
*Corresponding author. Email: mylesi@niaid.nih.gov
†These authors contributed equally to this work.

risk factors for AD. In addition to known impacts on human physiology, we propose that (di)isocyanates contribute to AD pathogenesis by shifting the physiology of health-promoting commensals toward disease phenotypes.

RESULTS

Carbon and nitrogen metabolism distinguishes health- and disease-associated strains of *R. mucosa*

We previously reported that microbial lipid production, particularly choline-containing glycerolipids, were essential for modeled therapeutic benefits of *R. mucosa* treatment (*8*). This is consistent with known benefits of the glycerolipid axis in skin health (*17*). However, the mechanisms underlying the differing lipid production between healthy volunteer (HV)– and AD-associated isolates were unknown. An initial metabolic phenotyping of HV- versus AD-associated isolates of *R. mucosa* was performed using the BioLog system (*18*), which tests which substance organisms are capable of metabolizing (Fig. 1A). The metabolites with the largest differential in their impact on the growth between HV- and AD-associated isolates were concentrated in the urea and citrate cycles (Fig. 1, B and C). HV-sourced isolates (*Rm*HV) had a greater boost in growth from supplementation with metabolites in glycolysis and the citric acid cycle, while AD-associated isolates (*Rm*AD) had greater growth enhancement with metabolites in the urea cycle (Fig. 1B).

Consistent with these findings, adenosine triphosphate (ATP; an inhibitor of the citrate cycle) more profoundly reduced the growth of *Rm*HV, while alanine (an inhibitor of the urea cycle) diminished *Rm*AD growth (fig. S1, A and B). Supplementation of the growth medium with *Candida* spp.–derived β-glucan (a carbohydrate) modestly enhanced the growth of *Rm*HV isolates (fig. S1C); meanwhile, *Rm*AD isolates metabolized the AD-associated antimicrobial peptide LL-37 (Fig. 1D) (*19*) and were less susceptible to its inhibitory effects (fig. S1D). However, despite *Rm*AD growth being less robust overall and more affected by nitrogen-containing LL-37 and alanine, *Rm*HV strains were capable of growing in medium devoid of fixed nitrogen, while *Rm*AD were not (Fig. 1E).

Health- and disease-associated strains of *R. mucosa* differ in CO_2 fixation and dependence

Growth without fixed nitrogen or with limited carbon in the culture medium raised the possibility that *R. mucosa* was fixing these elements from the atmosphere. To test this, we vacuumed the air out of an anaerobic chamber and replaced it with custom gas mixes (Fig. 1F). Atmospheric CO_2 concentration has increased since 1960 and has a similar seasonality pattern as AD (*20*, *21*). Placing isotopic CO_2 ($^{13}CO_2$) into the headspace, we found a small increase in total ^{13}C in most isolates, suggesting fixation (Fig. 1G). Flux analysis (which tracks the isotopic atoms as they travel through metabolic pathways) revealed that, for *Rm*HV, ^{13}C was preferentially incorporated into metabolites in the fatty acids and glycerolipid pathways, whereas *Rm*AD did not have any metabolic pathway with significant ^{13}C incorporation (Fig. 1H). In an inverse experiment, CO_2 was removed from the headspace; this affected the amino sugar and nucleotide sugar metabolism pathways in *Rm*HV, whereas *Rm*AD revealed alterations in butanoate, lysine degradation, and pentose and glucuronate interconversion pathways (Fig. 1H). In addition, *Rm*AD isolate morphology was more affected by removal of CO_2 from the headspace but the differences in growth were not statistically significant (Fig. 1, I and J).

Health- and disease-associated strains of *R. mucosa* differ in N_2 fixation and dependence

Like $^{13}CO_2$, $^{15}N_2$ was incorporated in both *Rm*HV and RmAD strains, albeit to a lesser extent than a closely related quintessential nitrogen fixer from plant biology, *Azospirillum brasilense* (Fig. 2A). Significant pathways indicated by flux analysis showed that both *Rm*HV and *Rm*AD isolates fixed N_2 into the cysteine and methionine pathway, while *Rm*HV additionally shuttled N_2 into α-linolenic acid (αLa) metabolism (Fig. 2B). Culture in N_2-free headspace revealed significant impact on the growth of only *Rm*HV (Fig. 2C). In *Rm*HV, N_2 deprivation significantly affected αLa, glutamine/glutamate, peptidoglycan biosynthesis, and fatty acid degradation; meanwhile, only butanoate and lipopolysaccharide (LPS) pathways were significantly affected in *Rm*AD (Fig. 2, D and E, and fig. S1, E and F). N_2 deprivation also generated a significant reduction in total annotated ceramides (Fig. 2F) and altered levels of several annotated lipids (fig. S1, G to O). *Rm*HV cultured in the absence of N_2 lost its modeled therapeutic benefit in mice (Fig. 2G). Pathway analysis of matrix-assisted laser desorption/ionization mass spectrometry imaging (MALDI-MSI) of the ear tissue (Fig. 2H) revealed that treatment with N_2-deprived *Rm*HV led to significantly less activation of the murine glycosaminoglycan degradation pathway and two glycerophospholipid pathways (Fig. 2, I to K).

Disease-associated *R. mucosa* ferment isopropyl alcohol under N_2 restrictions

To assess other atmospheric elements that *Rm*AD might use for respiration in lieu of nitrogen, we screened for production of the sulfur gases and methane, which would be indicative of sulfur-oxidizing bacteria and methanogens, respectively (fig. S2A) (*22*); each was negative (fig. S2B). *Roseomonas* produced acetate and lactate (fig. S2, C and D) and correlated with *Rm*HV generating pH values closer to those associated with healthy skin (fig. S2E) (*23*); however, isolates did not produce the hydrogen gas expected of true acetogens or lactogens (fig. S2B) (*22*). Instead, under N_2 deprivation, combustible gas was detected from *Rm*AD strains but not *Rm*HV (fig. S2B). Screening against known combustible gases revealed positive change in a detection tube, which reacts to both ethanol and isopropyl alcohol (fig. S2F); gas chromatography peaks were consistent with isopropyl alcohol while excluding ethanol (fig. S2, G and H). Together, our findings suggest that a pollutant of interest may circumvent N_2 fixation in *R. mucosa* by providing the ability to ferment isopropyl alcohol and preferencing lysine and/or butanoate pathways at the expense of the lipids necessary for therapeutic benefit (fig. S3A).

Traditional pollutants do not strongly associate with AD disease or commensal pathways

Initial tests of water contaminants that may affect nitrogen metabolism failed to identify any for which *Rm*AD appeared better adapted (fig. S3, B to F), did not consistently affect the pathways of interest (fig. S3G), nor induce N_2 independence (fig. S3H). revious work (*24*–*32*) identified subtle but statistically significant associations between AD and carbon monoxide (CO), particulate matter (PM), NO_X, and overall proximity to highways (Fig. 3A); however, these pollutants have been declining in atmospheric

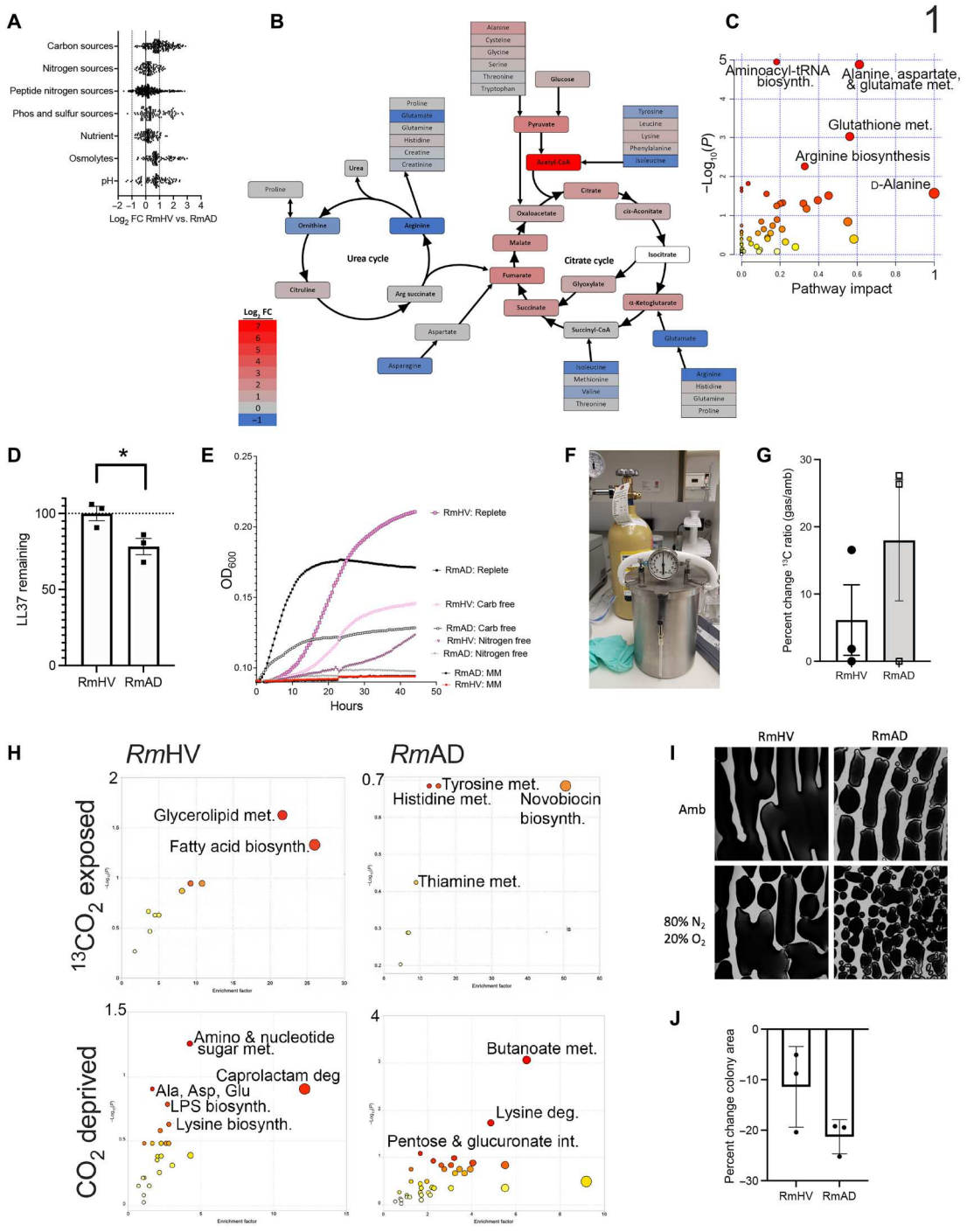

Fig. 1. *R. mucosa* from healthy controls shows differential carbon and nitrogen metabolism. (**A** to **J**) Three different isolates of *Roseomonas* from healthy volunteers (*Rm*HV1-3) and three different isolates of *Roseomonas* from patients with AD (*Rm*AD1-3) were grown in the BioLog system, fold change (FC) for each challenge condition versus control was calculated, the $\log_2$FC for *Rm*HV divided by the $\log_2$FC for *Rm*AD is shown (A), and then the ratio of $\log_2$FC was superimposed onto the urea cycle (arginine biosynthesis) and citrate cycle (alanine, aspartate, and glutamate metabolism; H). (B and C) Individual BioLog components were ranked by significance and analyzed for pathways by MetaboAnalyst. (D) *Rm*HV1-3 and *Rm*AD1-3 were cultured with known amounts of LL-37 for 24 hours; supernatants were collected and assessed for remaining LL-37 by ELISA and the percentage of input LL-37 signal calculated and displayed. (E) Absorbance for cultures of *Rm*HV1-3 or *Rm*AD1-3 in medium with no energy source [minimal medium (MM)], with only carbohydrate energy sources (Nitrogen free), with only amino acid energy sources (Carb free), or with both (Replete). (F) Picture of experimental setup where anaerobic chambers were evacuated before filling with custom gas mixtures. (G) Total change in ^{13}C to ^{12}C ratio for all *R. mucosa* isolates after 48 hours in culture supplemented with 1% $^{13}CO_2$. (H) MetaboAnalyst pathway analysis for *Rm*HV1-3 and *Rm*AD1-3 derived from metabolites with significant differences in ^{13}C to ^{12}C ratio after culture in 1% $^{13}CO_2$ or metabolites differentially affected in *Rm*HV by culture in ambient conditions or in CO_2 deprivation (80% N_2 and 20% O_2). (I and J) Representative image (1.25×) of culture morphology (I) and statistical enumeration (J) of area covered per imaging field by culture of *Rm*HV and *Rm*AD in ambient or CO_2 deprivation conditions. Data shown represent two or more independent experiments and are displayed as means ± SEM. For (C) and (H), only $-\log_{10} P$ values of >1 were considered significant.

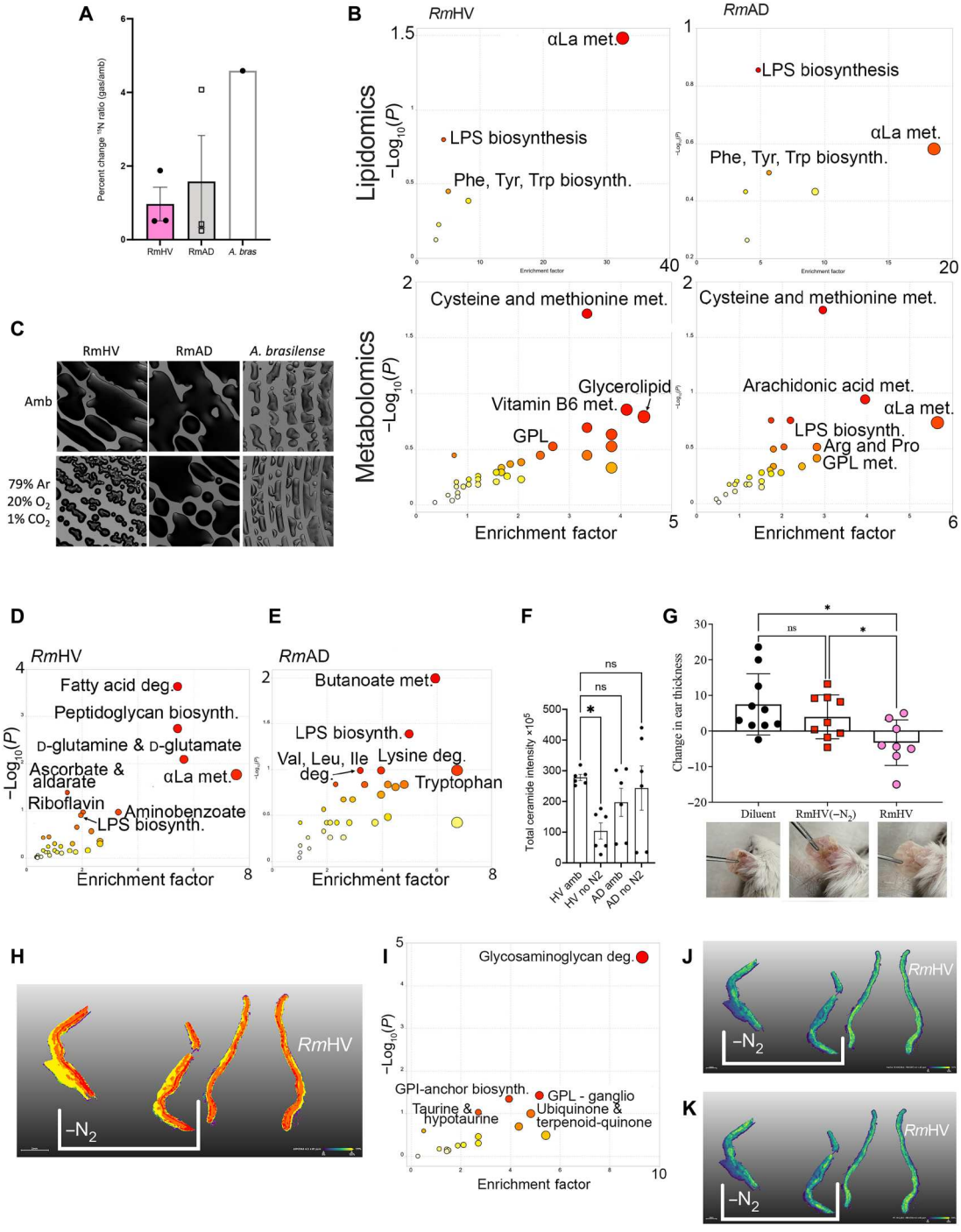

Fig. 2. *Roseomonas* isolates differ in nitrogen fixation. (**A**) Total change in ^{15}N to ^{14}N ratio for three isolates of *Roseomonas* from healthy volunteers (*Rm*HV1-3), three isolates of *Roseomonas* from patients with AD (*Rm*AD1-3), or one isolate of *A. brasilense* (*A. bras*) cultured with $^{15}N_2$ in head space. (**B**) Flux analysis was performed on metabolites with increase in ^{15}N ratios; metabolites with greatest ^{15}N change were ranked by *P* value and analyzed by MetaboAnalyst for pathways in lipidomic and metabolic acquisition conditions. (**C**) Representative images (1.25×) from spiral plated culture on agar for bacteria cultured in ambient air (Amb) or in head space devoid of N_2 [79% argon (Ar), 20% oxygen (O_2), and 1% carbon dioxide (CO_2)]. (**D** and **E**) *R. mucosa* metabolites most affected by N_2 deprivation were assessed by MALDI–time-of-flight (TOF) MS and analyzed for pathways affected by MetaboAnalyst. (**F**) Total intensity values for annotated ceramide containing compounds assessed by MALDI. (**G**) Mice treated in the MC903 model of AD for 8 days of dermatitis induction, 3 days of treatment with either *Rm*HV cultured in ambient conditions of N_2 deprivation ($-N_2$), and then 4 days of observation; change in mouse ear thickness between days 8 and 15 is shown. Reduced thickness indicates reduced swelling and improved outcomes. (**H**) MALDI-MSI performed on mouse ears; segmentation performed by SCiLS Lab. (**I**) Pathway analysis derived from metabolites that best distinguish mice ears treated with *Rm*HV1 from ambient conditions versus treatment with *Rm*HV1 cultured in N_2 deprivation. (**J** and **K**) Distribution of indicated metabolites as indicated by MALDI-MSI. GPL, glycerophospholipids; GPI, glycerophosphatidylinositol; deg., degradation; αLa, α-linolenic acid. Data shown represent two (G to K) or three or more (A to F) independent experiments. *$P < 0.05$; ns, not significant as determined by ANOVA.

concentration during the time of rising AD rates (*33*). Furthermore, challenging *Rm*HV with traditional car exhaust exposures failed to consistently affect growth or differentially affect therapeutic pathways (Fig. 3B and fig. S4, A to D).

Diisocyanates strongly associate with AD diagnosis rate

To produce an untargeted screen for environmental exposures, we first mapped the rate of AD diagnosis among total billed clinic visits by U.S. zip codes (Fig. 3C). Cluster analysis collated zip codes by their relative risk of having an above-average rate of AD diagnosis rate for 2019 (Fig. 3D). Next, we contrasted these data with the cumulative exposures reported in the Environmental Protection Agency's (EPA) Toxic Release Inventory (TRI) from 2014 to 2019. The TRI includes industry self-reported data on the environmental release of over 500 chemicals that may be released into the environment in three different ways: into the water, ground-level atmospheric release (fugitive), or pumped through a chimney (stack). Numerous models were constructed using the TRI, AD rates, and potential confounders such as obesity [which encourage allergic priming primarily through inhibition of short-chain fatty acid production by gut organisms (*34*)], poverty (which affect access to medical care in general), and access to specialty care (local numbers of pediatricians, allergists, or dermatologists). Because each zip code lacked most of the TRI pollutants, the overall similarity of zip codes was high and failed to segregate by AD rate (fig. S4E).

However, unraveling the cumulative exposure to specific pollutants using the lasso-penalized multivariate Poisson regression model indicated that fugitive diisocyanate release and population density were the most predictive indicators beyond access to providers (Fig. 3E). Additional models revealed that diisocyanates were also the top environmental exposure identified by univariate Poisson regression (fig. S4F), by lasso selection across multiple years (fig. S4G), and by random forest (Fig. 3F). The partial dependence plot for fugitive TDI and other diisocyanates demonstrated a monotonic increase (Fig. 3G), consistent with the anticipated associations like population density and specialist access (fig. S4H). Because children are less likely to have migrated away from their place of birth than adults, we sub-analyzed only visits to pediatricians and found that the impact of diisocyanates was even more prominent (Fig. 3H and fig. S5A). The impact of diisocyanates on pediatric AD was also seen using the more advanced EPA database Risk-Screening Environmental Indicators (RSEI) (Fig. 3I). Using the regression correlation coefficients for each significant exposure (fig. S5A) to aggregate an AD-associated exposure score revealed that zip codes with scores of ≤1 SD below the mean had a 7.7-fold lower pediatric visit rate than those with scores of ≥1 SD (Fig. 3J) and significant linear relationship when either averaged by decile (R^2 = 0.97) or used as an internal predictor (R^2 = 0.93; fig. S4, I and J).

Diisocyanates continued to be among the highly associated variables in related atopic diseases in children such as peanut allergy, general atopy, and asthma (fig. S5, B to D), but not allergic rhinitis (fig. S5E). Airborne diisocyanates were not associated with clinic visits for psoriasis (fig. S5F) and were not among the many neurotoxic chemicals associated with autism or schizophrenia diagnoses (fig. S5, G and H)—diseases related to AD only in a shared association with industrialization and findings of dysbiosis (*35*–*37*).

TDI affects therapeutic pathways in *R. mucosa*

Consistent with the timing of rising AD rates in the United States, production of the two main diisocyanates rapidly increased starting in the mid- to late-1970s (Fig. 4A) (*38*). Methylene diphenyl diisocyanate (MDI) and toluene diisocyanate (TDI) are the most common industrial diisocyanates manufactured for a variety of downstream products like furniture cushions, nylon, paint, polyurethane, and adhesives (*25*); many such products are associated with the increased risk of AD (Fig. 3A). Although AD rates and TDI production were only available for eight countries, a significant linear correlation was seen between annual TDI production and average AD rates for children under 14 years of age (Fig. 4B). The reported fugitive releases for various diisocyanates in the United States ranged from 0.52 mg/hour to 1157 g/hour (means, 2.5 to 31 g/hour; medians, 41.9 to 973 mg/hour; Fig. 5C). MDI is nonvolatile unless modified and did not differentially affect growth (fig. S6A), N_2 dependence (fig. S6B), or relevant metabolic pathways (fig. S6C).

However, 1.2 mg of TDI placed in the culture dish lid released a mean of 137 ng/hour, which is well below the average annual reported release by factories into the atmosphere (Fig. 4C). *Rm*HV colonies closest to the TDI were inhibited (fig. S6D), while colonies outside of the zone of inhibition demonstrated enhanced growth and N_2 independence (Fig. 4D). Calculated exposures as low as 7 to 30 parts per trillion (ppt) affected growth, inhibited production of total ceramides (Fig. 4, E and F), and altered production of several other lipids (fig. S6, E to L) in ways that are consistent with the known impact of isocyanates on amine-containing lipids (*39*, *40*). In *Rm*HV, TDI affected the previously identified N_2-dependent beneficial pathways, including αLa, LPS, and amino-nucleo sugar metabolism (Fig. 4G and fig. S6M). Although temperature sensitive, a common air purifier was able to reduce the levels of TDI in a standard sized room from 1.5 parts per billion (ppb) to below detectable levels (<0.5 ppb; fig. S6N) but was unable to protect *R. mucosa* from TDI impacts on growth or ceramide production (fig. S6O). Similar to *Rm*AD metabolism (fig. S2B), *Rm*HV exposed to TDI produced combustible gas under N_2 deprivation (Fig. 4H). Furthermore, unlike toluene, exposure to TDI negated the modeled benefit of *Rm*HV treatment in mice (Fig. 4I), suggesting a specific activity of the cyanate groups.

HNCO affects therapeutic pathways in *R. mucosa*

To further elucidate the impacts of the cyanate groups, we next tested HNCO (also called isocyanic acid). HNCO is also a component of several exposures linked to AD severity (Fig. 3A) (*31*, *41*) such as the smoke from wildfires, environmental tobacco smoke, as well as gasoline exhaust when burned through the catalytic converters that were introduced in the United States in 1975 (*26*, *27*, *42*–*45*). Like TDI, HNCO altered growth, generated N_2 independence (Fig. 5A), induced isopropyl alcohol from N_2-deprived *Rm*HV (Fig. 5B), and negated therapeutic benefit in mice (Fig. 5C). HNCO also affected relevant cell wall pathways including amino-nucleo sugars and peptidoglycans in *Rm*HV (Fig. 5D and fig. S6, P and Q).

Diisocyanate-containing glue, but not plant-based glue, altered growth (Fig. 5E), produced N_2 independence (Fig. 5F), and affected LPS metabolism (Fig. 5G and fig. S6R). Meanwhile, polyurethane-based glue affected αLa and enhanced the growth of *Rm*AD (Fig. 5, H to J). Both glues released diisocyanates at levels consistent with

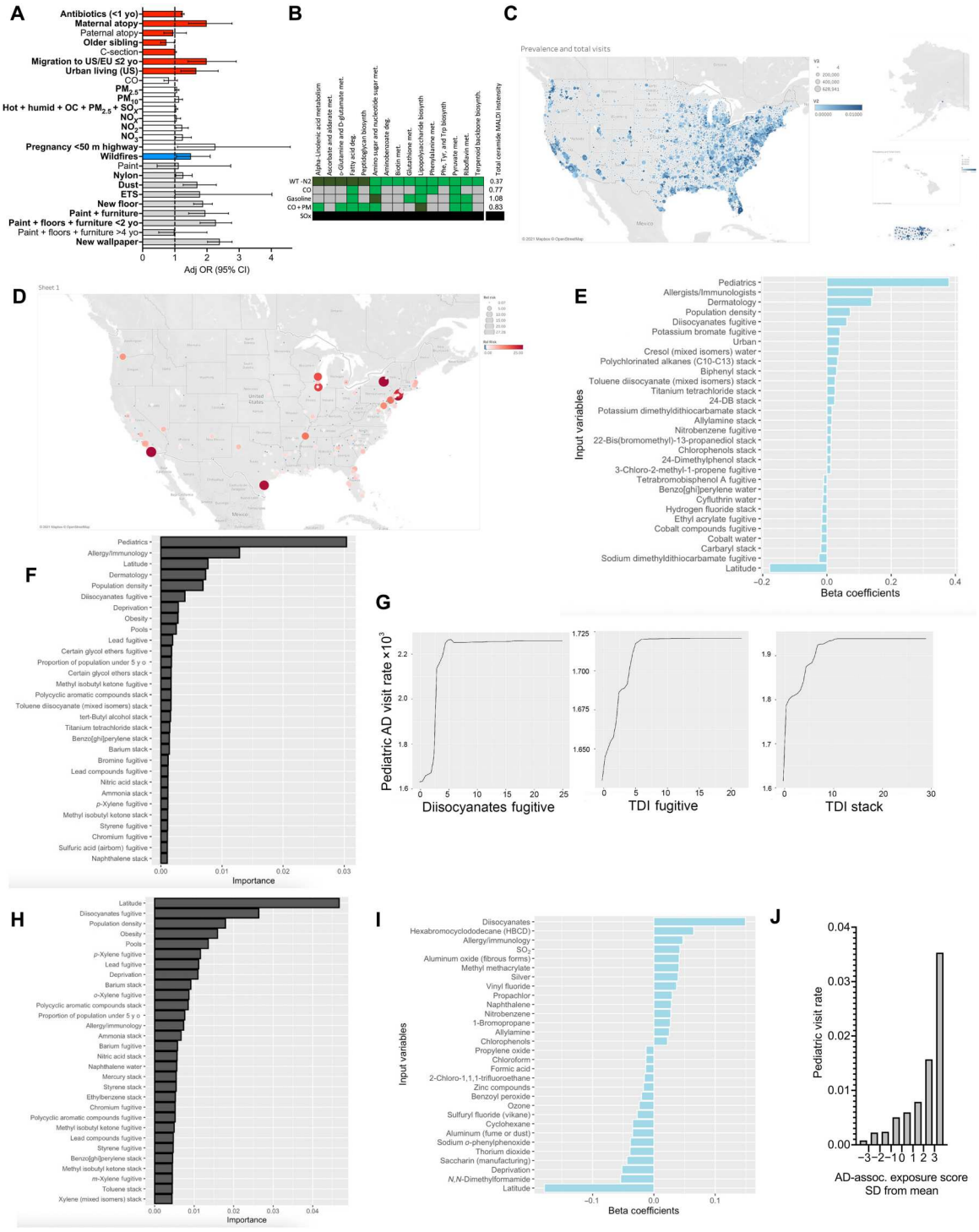

Fig. 3. Diisocyanates associated with AD diagnoses. (**A**) Summary of published environmental factors influencing AD (*6*, *24*, *26*–*32*, *41*, *42*). Migration from developing to United States or European Union nations (US/EU); PM, particulate matter; ETS, environmental tobacco smoke; OC, organic carbon; OR, odds ratio; CI, confidence interval. (**B**) *Rm*HV was cultured in sealed chamber with trace CO, CO + PM, SO_2, or gasoline in agar dish lid and compared to pathways modified by N_2 deprivation; green indicates that the MetaboAnalyst identified pathway was altered by chemical challenge; dark green indicates significant alteration; black indicates that no growth was evident. (**C**) Raw values and diagnosis rate for AD by zip code. (**D**) Cluster analysis for relative risk of having above-average AD diagnosis rate. Regression was performed for 1500+ pollution variables from the EPA TRI, AD diagnosis rates, obesity, deprivation index, and access to pediatricians, allergists, or dermatologist. (**E** to **G**) Linear regression using lasso with 1 SE limitation (E), random forest (F), or partial dependence plots (G) for total release values from 2014 to 2019 versus 2019 visit rates. (**H**) Random forest as in (F) but restricting to only billings by pediatricians. (**I**) Lasso linear regression with 1 SE for total 2019 pediatric visit rates versus 2014–2019 release values from the RSEI EPA database. (**J**) Aggregate AD-associated pollutant scores were summated by zip code for each pollutant multiplied by its β correlation value; mean values for each SD section were indicated.

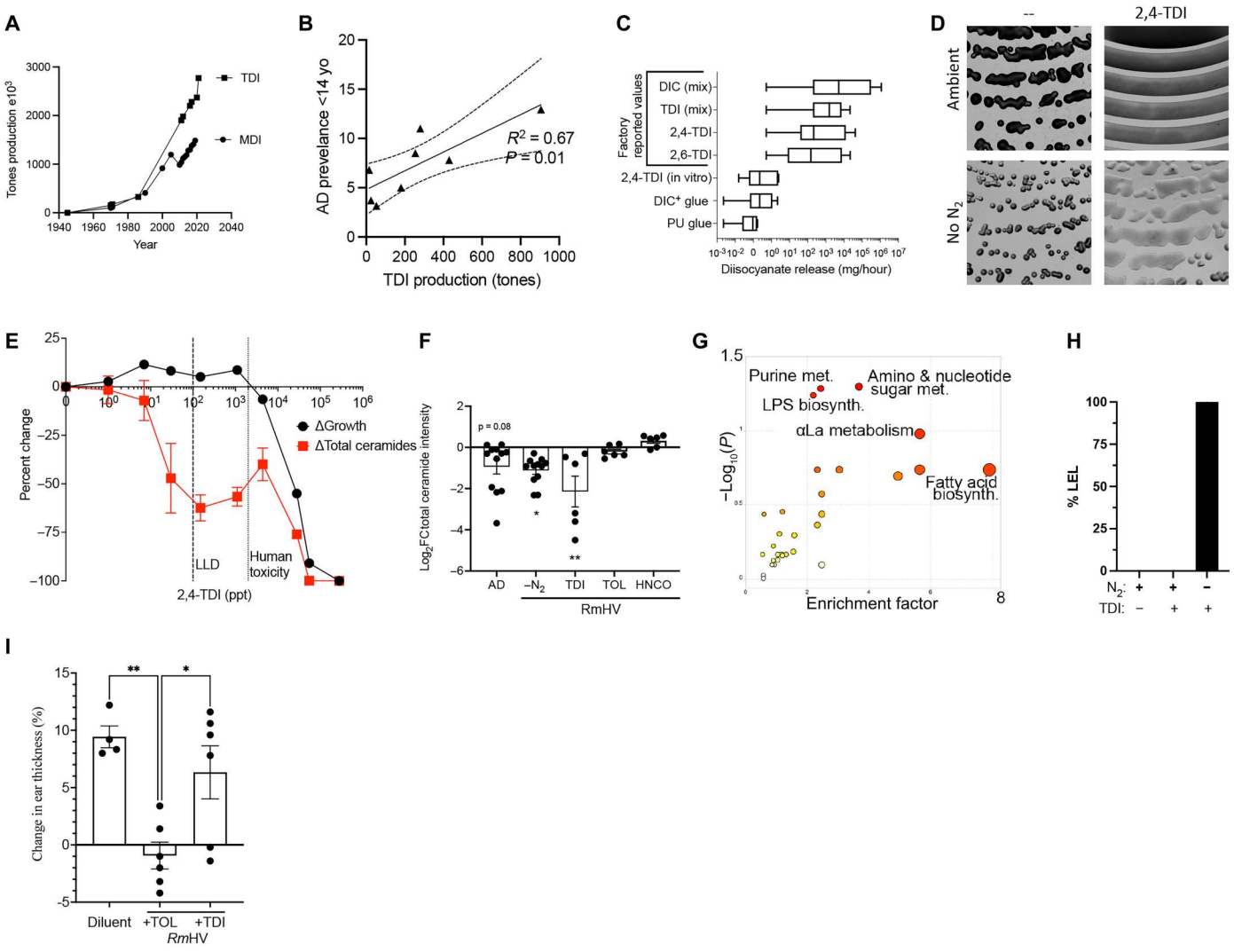

Fig. 4. TDI disrupts beneficial pathways in *R. mucosa*. (**A**) Total U.S. production of TDI and MDI since 1940. (**B**) The 2019 TDI production for nations with available data in linear regression with 95% confidence intervals against reported rates of AD in children under 14 years of age. (**C**) Detected levels of diisocyanates (DIC) including TDI released during in vitro experiments compared to reported factory release. (**D**) Representative image (1.25×) of *Rm*HV1-3 cultured with TDI in ambient or N_2 deprivation conditions. (**E**) TDI was measured at serial dilutions so that values at higher dilutions below the lower limit of detection (LLD) could be extrapolated. Percent change in growth and total intensity of annotated ceramides by MALDI at 48 hours are shown. (**F**) Change in total intensity for annotated ceramides as compared to *Rm*HV1-3 cultured in ambient conditions or *Rm*AD1-3 in ambient conditions (AD) or *Rm*HV under N_2 deprivation ($-N_2$), or with TDI, toluene (TOL), or HNCO. (**G**) MetaboAnalyst indicated affected pathways in *Rm*HV1-3 by culture with TDI or toluene. (**H**) Lower explosive limit (LEL) detection for *Rm*HV1-3 with and without TDI exposure in ambient or N_2 deprivation. (**I**) Mice treated in the MC903 model of AD before treatment with either diluent or *Rm*HV1 grown with toluene or with TDI; change in mouse ear thickness is shown. Data shown are representative of three or more independent experiments and shown as means ± SEM. $^*P < 0.05$, $^{**}P < 0.01$ as determined by ANOVA.

reported factory releases (Fig. 4C). Together, these data suggested that isocyanate exposure may induce N_2 independence in *Rm*HV by providing the ability to ferment isopropyl alcohol at the expense of producing the lipids necessary for therapeutic benefit.

Improvement in AD with *R. mucosa* treatment is influenced by TDI exposure

Building upon prior open-label safety and activity of topical *R. mucosa* (*8*, *9*) a 15-site, placebo-controlled phase IIb trial in 154 patients aged 2 to 70 years was performed under a National Institutes of Health (NIH) license by Forte Biosciences Inc. (Table 1). In the 2-week lead before enrollment, patients were provided a moisturizer regimen with minimal dysbiotic potential (*16*) and instructed to discontinue topical corticosteroids (TCS) throughout the study. Then, patients were treated three times per week for 4 months, followed by a 1-month washout in which both topical steroids and the preset moisturizers were withheld (fig. S7A).

The only serious adverse event during the trial was an unrelated appendicitis in one patient (Table 2); the subject was an 8-year-old male who developed abdominal pain 3 weeks into active therapy. A week later, he went to the emergency room, was diagnosed with appendicitis by abdominal imaging and exam, and underwent a successful appendectomy. White blood cell counts were within normal limits, and the appendix was not ruptured before removal. He was given cefoxitin while in the hospital and discarded the following day. He then resumed therapy and completed the trial without

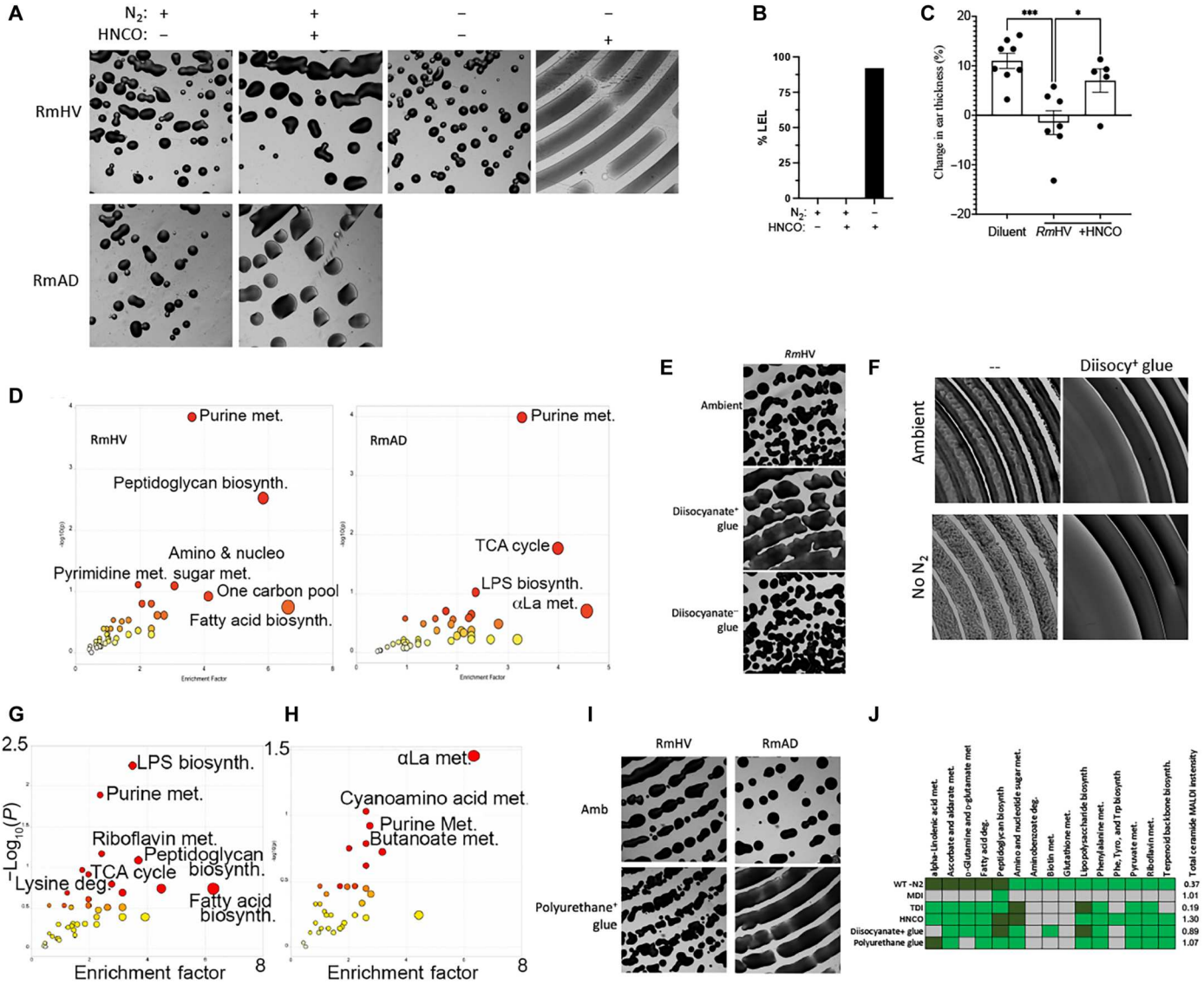

Fig. 5. HNCO disrupts beneficial pathways in *R. mucosa*. (**A**) Representative image of *Rm*HV1 cultured with 1 μg of HNCO placed into the lid of the agar dish and cultured for 48 hours in ambient or N_2 deprivation conditions. (**B**) Lower explosive limit (LEL) detection by gas monitoring for *Rm*HV with and without HNCO exposure in ambient or N_2 deprivation culture conditions. (**C**) Change in mouse ear thickness during MC903 model of AD for mice treated with *Rm*HV1 in ambient conditions or exposed to HNCO. (**D**) MetaboAnalyst pathway analysis for metabolites affected in *Rm*HV1-3 or *Rm*AD1-3 cultured with HNCO in the lid of agar dish. (**E**) Representative image of *Rm*HV1-3 cultured with diisocyanate-containing glue or corn starch–based diisocyanate-negative glue placed into the lid of the agar dish and cultured for 48 hours. (**F**) Representative image of *Rm*HV1-3 cultured with diisocyanate-containing glue placed into the lid of the agar dish and cultured for 48 hours in ambient or N_2 deprivation conditions. (**G** and **H**) MetaboAnalyst pathway analysis for metabolites affected in *Rm*HV1-3 cultured with diisocyanate-containing glue (G) or polyurethane-based glue (H) in the lid of agar dish. (**I**) Representative image of *Rm*HV1-3 and *Rm*AD1-3 cultured with polyurethane-based glue placed into the lid of the agar dish and cultured for 48 hours. (**J**) Summary table of *Rm*HV1-3 pathways affected by N_2 deprivation compared to pathways affected by indicated challenges along with fold change of total annotated ceramide containing metabolites; green indicates pathway affected per MetaboAnalyst, while dark green indicates significant impact and gray indicates pathway not affected. All images in (A), (E), (F), and (I) were taken at ×1.25 magnification. Data shown are representative of three or more independent experiments and shown as means ± SEM. *P < 0.05 and **P < 0.01 as determined by ANOVA.

further complication. Application site reactions were the only related complication but were neither severe nor more frequent than in the placebo group (Table 2). The study failed to meet the prespecified intention to treat (ITT) end points with no significant differences seen between the treatment and placebo group for the proportion reaching an investigator global assessment (IGA) of clear or almost clear or the percent change from baseline in the Eczema Area and Severity Index (EASI) at the end of active treatment (Fig. 6, A to C). However, before the onset of the coronavirus disease 2019 (COVID-19) pandemic, the U.S. Food and Drug Administration (FDA) was in the process of updating their metrics (*46*) with the acknowledgment that these end points do not account for the potential for colonization with probiotics to provide the long-term benefits sought by patients (*8*).

To understand whether treatment with *R. mucosa* might provide a more long-lasting benefit than placebo, we sub-analyzed those

Table 1. Characteristics of the patients enrolled in the clinical trial.

Characteristics	Treatment (*n*, %)	Placebo (*n*, %)	*P*
Sex			
Female (*n*, %)	42 (55.3)	46 (59)	0.64
Male (*n*, %)	34 (44.7)	32 (41)	
Ethnicity			
AIAN/NHPI (*n*, %)	2 (2.6)	0	0.81
Asian (*n*, %)	7 (9.2)	11 (14.1)	
Black (*n*, %)	18 (23.7)	15 (19.2)	
White (*n*, %)	46 (60.5)	48 (61.5)	
Multiple (*n*, %)	3 (3.9)	4 (5.1)	
Age (years)			
Mean (SD)	17.2 (16.6)	16.8 (16.5)	0.88
Median	12	12	1.0
Range	2–70	2–69	
2–11 year olds (*n*, %)	37 (48.7)	38 (48.7)	1.0
12–17 year olds (*n*, %)	22 (28.9)	23 (29.5)	
>18 years (*n*, %)	17 (22.4)	17 (21.8)	
Severity			
IGA 2 (*n*, %)	10 (13.2)	12 (15.4)	0.69
IGA 3 (*n*, %)	66 (86.8)	66 (84.6)	
EASI (mean, SD)	10.2 (3.66)	9.6 (3.9)	0.33
BSA (mean, SD)	13.4 (7.59)	12 (7.09)	0.23
Pruritus NRS (mean, SD)	5.3 (2.09)	5.3 (2.18)	1.0
POEMS (mean, SD)	13.5 (6.63)	13.4 (6.39)	0.92

Table 2. Summary of all adverse events reported during the trial.

	Treatment (*n*, %)	Placebo (*n*, %)	*P*
Treatment emergent adverse events			
Total participants with ≥1	16 (21.1)	16 (20.5)	0.93
Related, likely related, or possibly related			
Administration site conditions			
Site pain	4 (5.3)	2 (2.6)	0.5
Site pruritus	1 (1.3)	0	
Site urticaria	1 (1.3)	0	
Contact dermatitis	0	2 (2.6)	
Unrelated			
Hypothyroidism	0	1 (1.3)	1.0
Lacrimation increase	1 (1.3)	0	1.0
Gastrointestinal			
Abdominal pain	0	1 (1.3)	1.0
Diarrhea	0	1 (1.3)	1.0
Vomiting	1 (1.3)	0	1.0
Seasonal allergies	0	1 (1.3)	1.0
Infections			
Appendicitis (*severe AE)	1 (1.3)	0	1.0
Blister infection	0	1 (1.3)	1.0
Folliculitis	1 (1.3)	0	1.0
Gastroenteritis, viral	0	1 (1.3)	1.0
Molluscum contagiosum	1 (1.3)	0	1.0
Nasopharyngitis	1 (1.3)	0	1.0
Sinusitis	1 (1.3)	0	1.0
Tinea versicolor	0	1 (1.3)	1.0
Upper respiratory tract infection	1 (1.3)	1 (1.3)	1.0
Injury	4 (5.3)	4 (5.1)	1.0
Musculoskeletal			
Arthralgia	1 (1.3)	1 (1.3)	1.0
Back pain	2 (2.6)	0	0.3
Bone lesion	1 (1.3)	0	1.0
Groin pain	0	1 (1.3)	1.0
Osteochondrosis	0	1 (1.3)	1.0
Headache	0	1 (1.3)	1.0
Sciatica	0	1 (1.3)	1.0
Anxiety/depression	0	1 (1.3)	1.0
Asthma	0	1 (1.3)	1.0
Rhinorrhea	1 (1.3)	0	1.0
Ingrown nail	0	1 (1.3)	1.0

completing the entire study without TCS use (n = 117). This revealed either a significant or trend toward loss of the placebo/vehicle effect during the washout; whereas, similar to the open-label phase (*8*), treatment discontinuation did not lead to significant loss of efficacy in the active treatment group (Fig. 6D). By the end of the study, treatment had led to significant improvements in total EASI reduction in this subgroup (Fig. 6E) along with statistical trends toward improvement in the percent of patients achieving a 90% improvement (EASI90) (Fig. 6F). The EASI75 continued to increase after discontinuation, whereas the placebo group expectedly saw a loss of activity (Fig. 6G).

Further, post hoc stratification of clinical response by the study sites′ historical TDI exposure revealed that areas with above-average levels of TDI had a nonsignificant increase in baseline severity (fig. S7B) but were more responsive to *R. mucosa* treatment (Fig. 6, H to K) despite no statistical correlation between baseline severity and clinical improvement (fig. S7C). Although both treatment groups experienced a significant reduction in itch, the difference between them was not statistically significant (Fig. 6L). Like EASI response, TDI exposure significantly altered itch relief in the active treatment group (Fig. 6L). Although not indicative of prescription approval, under a consideration of over-the-counter use, we tested an encapsulated probiotic form of *Rm*HV for stability (fig. S7D) and

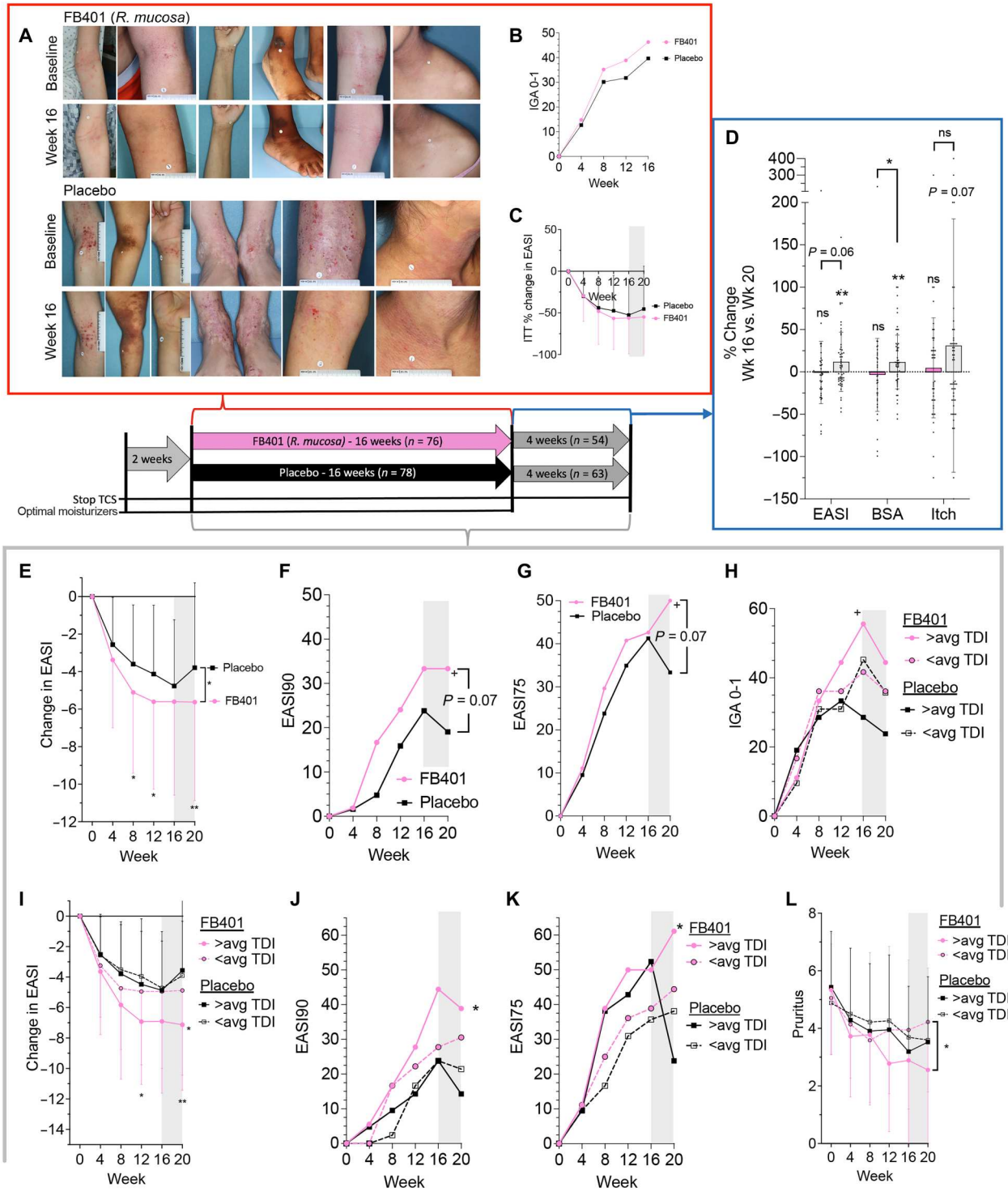

Fig. 6. Clinical results from *R. mucosa* treatment were influenced by TDI exposure. Patients were treated with topical *R. mucosa* (FB-401) or placebo (sucrose in water) thrice weekly for 16 weeks before a 4-week washout. Two weeks before treatment, topical corticosteroids (TCS) were stopped and a minimally dysbiotic moisturizer regiment was initiated. (**A**) Example images from participants. (**B**) ITT analysis for those achieving an IGA of 0 and 1 (**C**) and percent change in EASI during active treatment. (**D**) For those completing the washout phase, percent change between week 16 and week 20 as a percentage of enrollment values is shown for EASI, BSA, and pruritis NRS (itch); each dot represents one participant. (**E** to **L**) For those completing the entire 20-week trial without topical steroids, raw EASI change (E), the proportion achieving 90% improvement in EASI (EASI90; F), and EASI75 (G). (H to L) Post hoc stratification of the completer population results by study sites' historical TDI exposure as above the mean (>avg) or below for IGA0-1 (H), raw EASI (I), EASI90 (J), EASI75 (K), and pruritus (L); significance indicated for FB-401 in above or below average TDI zip codes against matched control unless indicated. Data are shown as proportion (B, F to H, J, and K) and means + SD (C, D, I, and L). ns, not significant, $^{+}P < 0.1$; $^{*}P < 0.05$; $^{**}P < 0.01$ as determined by ANOVA (C and D), rANOVA (E, I, and L), or chi-square (B, F to H, J, and K).

expanded our prior evaluation of products (*16*) into which *Rm*HV could be viably reconstituted (fig. S7E).

Isocyanates affected commensal staphylococcal species

Like *R. mucosa*, coagulase-negative *Staphylococcus* spp. can be protective against AD (*47*, *48*) and therefore presents an additional assay for the impacts of isocyanates. *Staphylococcus epidermidis* enhances host ceramide production and subsequent barrier function through production of sphingomyelinases (*48*). TDI exposure significantly altered *S. epidermidis*–induced glycerophospholipid metabolism and reduced total ceramide accumulation in human primary keratinocyte cultures (fig. S8, A and B). *Staphylococcus cohnii* improves outcomes in mouse models of AD by altering host metabolism but primarily affects steroid pathways rather than ceramides (*47*). We reproduced the reported murine benefits of *S. cohnii* and further identified potential synergy with *Rm*HV (Fig. 7A). Also consistent with prior reports (*47*), we identified the importance of steroid-related metabolism such as the primary bile acid and terpenoid backbone pathways in *S. cohnii* treatment (Fig. 7, B and C). However, it should be noted that unlike *Rm*HV (*49*), *S. cohnii* was able to generate organ infection in mice (fig. S8C) and thus should be considered skeptically if treating children with disrupted skin barrier function.

In HV-sourced *Staphylococcus*, isocyanates had differing impacts on amino-nucleo sugar and terpenoid backbone metabolism as well as many of the pathways that distinguished health from AD-associated isolates in culture (Fig. 7D and fig. S8D). Meanwhile, polyurethane and HNCO exposure did not differentially affect growth like TDI but had more pronounced impact on metabolic pathways (Figs. 7D and 8, A and D, and fig. S8, E to G). Traditional pollutants did not generate differential impacts on growth (Fig. 8A) and only CO, especially when combined with PM, affected important staphylococcal metabolic pathways (Fig. 7D and fig. S9, A to E). Like *Rm*HV, exposure to (di)isocyanate negated the significance of modeled benefit of *S. cohnii* treatment in mice (Fig. 8E).

Lysine protects commensal organisms from the impact of diisocyanates

As a means of protection from cationic antimicrobial peptides and oxidative stress, *S. aureus* up-regulates lysine synthesis and enzymatically attaches it to phosphatidylglycerol (PG) to make lysyl-PG (LysPG) (*50*). Given the propensity of (di)isocyanates to react with the amine groups on lysine (*51*), we hypothesized that increased lysine could also protect organisms against (di)isocyanates. As expected, AD-associated *Staphylococcus* had higher levels of LysPG than CoNS (Fig. 8F). While *R. mucosa* lacked detectable LysPG, AD-associated isolates demonstrated increased activation of the lysine biosynthesis pathway (fig. S9F). Pretreatment in lysine-supplemented culture medium partially negated the growth and metabolic impacts of TDI exposure for both *S. cohnii* and *Rm*HV (Fig. 8, G and H) while also preserving total ceramide production in *Rm*HV in a dose-dependent fashion (Fig. 8I and fig. S10).

DISCUSSION

For every organ system, there are both acute and chronic exposures for which the normal, expected response is organ dysfunction; with high enough exposures to particulate matter, radiation, or lead, the resultant pulmonary, hematologic, or neurologic harms each respectively become anticipated. When applied to mice, this reality is used by biomedical researchers all over the world. While genetic manipulation may be required for some models, most often noxious chemical stimuli are used to induce disease models in otherwise normal wild-type mice.

Reliably inducing disease in mice allows preclinical interventions to serve as preambles to human clinical trials during drug development. However, while the ability to reliably induce disease in mice is seen as an indication that the murine physiology is normal, the existence of the same disease in humans is often approached as an indication that the patient's physiology must be abnormal. TDI and the related hexamethylene diisocyanate (HDI) represent two of the small number of chemicals capable of inducing AD models in mice through a T helper cell 2 (T_H2)/TARC-mediated mechanism that is amenable to established AD treatments like TCS, Janus kinase (JAK) inhibitors, and PDE4 inhibition (*52*).

A construct in social science called the groundwater approach asks one to imagine coming across a lake with only one or two fish floating dead in the water; in such a scenario, "it makes sense to analyze the fish" (*53*). But if one were to come upon a lake with 20% of the fish floating dead, you would innately know that you need to both "analyze the lake" (*53*) and stay out of the water. Since 1970, the pediatric incidence of AD in the United States has risen from approximately 2 to 5% to 15 to 20% (*2*). Here, we propose that diseases strongly linked to industrialization, such as AD, may in part be an anticipatable consequence of being nursed in the polluted waters of this analogy.

Industrialization is the principal component predicting speciation of the gut microbiome (*54*). Although less extensively evaluated, the skin microbiome also demonstrates more subtle differences in speciation between different environments (*55*). While humans have only had approximately 10 generations to adapt to the industrial revolution and even fewer to the exposome of the last half century, commensal microbes have had over a million generations since 1950 alone. In this report, we propose a paradigm for research, which suggests that dysbiosis recapitulates environment.

Our work suggests that the dysbiosis seen in AD may be related to (di)isocyanates: Diisocyanates were the industrial toxin most strongly correlated with AD clinical visits; manufacturing of diisocyanates is temporally related to the rise of AD; epidemiologic factors previously linked to AD would each increase exposure to (di)isocyanates; AD-associated isolates appear to be better adapted to surviving diisocyanate exposure; and the pathways needed for therapeutic benefit in commensal strains of *R. mucosa*, *S. epidermidis*, and *S. cohnii* are adversely affected by (di)isocyanates. Furthermore, the advantages of microbial transplantation were more evident in areas where the native microbiota would be expected to be affected by TDI. We interpret this finding as a suggestion that replenishing the microbiome with *Rm*HV may be of greater benefit when patients are expected to have TDI-altered microbiota. However, prospective studies will be required for such assessments and to evaluate whether local TDI levels could adversely affect the longevity of *Rm*HV by toxifying the treatment strains.

Beyond microbially mediated effects, further work into diisocyanate exposure may elucidate some host biomarkers of AD, which currently lack clear etiologies. For example, the deficiencies in amine-containing lipids in patients with AD (*56*) are consistent

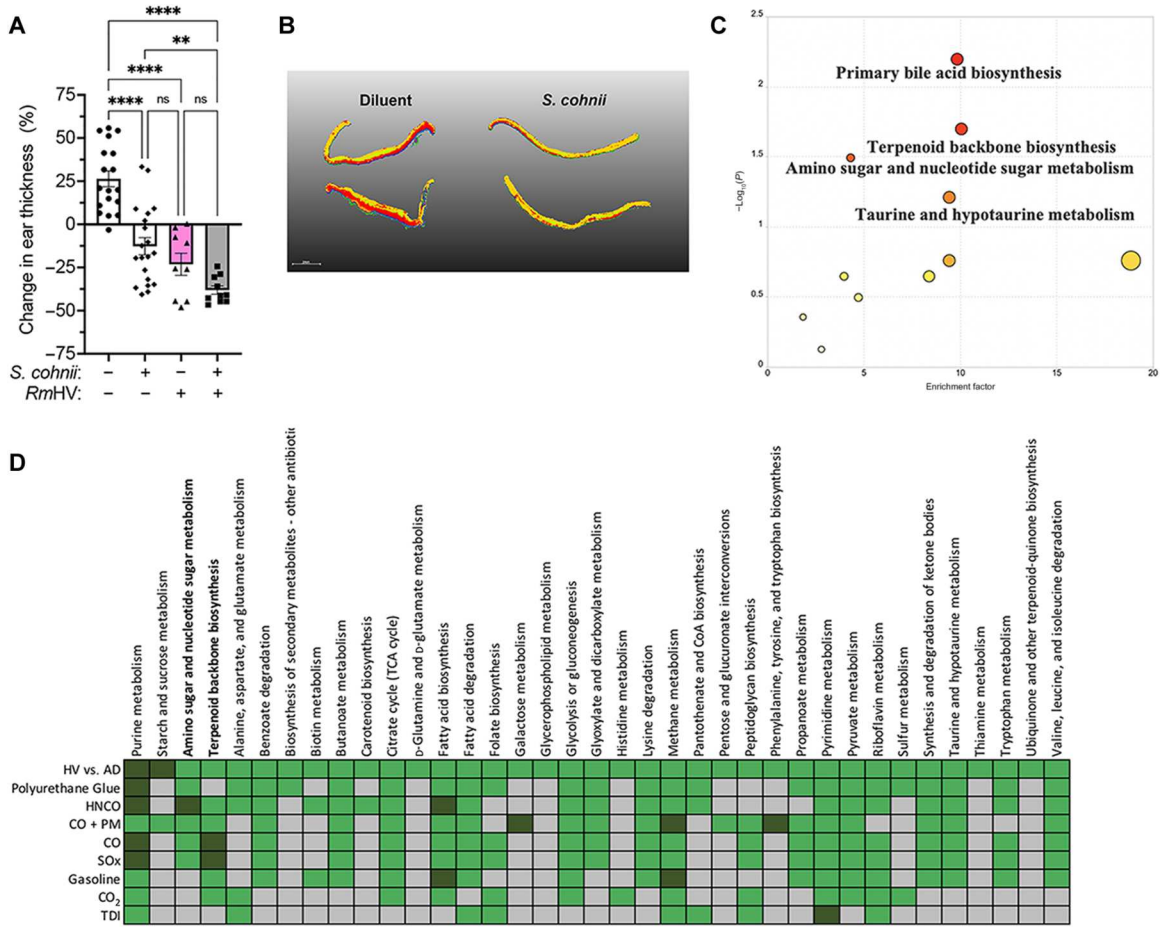

Fig. 7. *S. cohnii* improves outcomes in mouse models of AD via steroid metabolism. (**A**) Mice treated in the MC903 model of AD before treatment with either diluent or *S. cohnii*. (**B**) Segmented MALDI-MSI performed on mouse ears. (**C**) MetaboAnalyst pathways affected on mouse ears treated with *S. cohnii*. (**D**) Summary table of MetaboAnalyst pathways differentiating isolates of *Staphylococcus* spp. from healthy volunteers (*Staph* HV) versus isolates of *S. aureus* from patients with AD (*Staph* AD); green indicates that the pathway was affected, dark green indicates significant impact, and gray indicates not affected.

with carbamoylation of amine groups by (di)isocyanates (*51*). The itch-inducing, T_H2-responsive thermoreceptor TRPA1 is up-regulated in AD models and directly activated by TDI (*57*). The autoreactive immunoglobulin E (IgE) and autoreactive T cells seen in patients with AD (*58*) should be reevaluated in the context of (di)isocyanate's ability to promote autoreactivity to host proteins via haptinization (*39*). Such studies may elucidate whether AD pathogenesis includes (di)isocyanate-mediated proimmunogenic haptenization or neurologic priming during early-stage development.

Overall, our research performed a hazard assessment for isocyanates and AD while also presenting a microbiome-mediated mechanism. To our knowledge, this is the first report demonstrating that pollution may promote disease by disrupting metabolism in commensal microbiota. In its currently stage, our work is limited by its correlative nature. However, epidemiologic data suggest that the environmental risk factors for AD may predominate before age 4 years (Fig. 3A). This early-age restriction of risk combined with the known (*59*) and proposed hazards of diisocyanates precludes ethical use of challenge models for AD development. Therefore, our data should instead endorse actionable follow-up for longitudinal monitoring of ambient (di)isocyanates along with concurrent tracking of local AD prevalence and severity to assess our population findings at the level of individual patients. Once individual patients can be assessed, odds ratios and/or relative risks for each level of AD severity should be calculated.

Performing subsequent environmental exposure and dose-response assessments will be challenging given that the current detection and filtration systems are calibrated to indoor, industrial-level exposures relevant only for adults who would be outside the critical age window for AD development (*6*, *42*). However, if detection systems capable of assessing at ppt concentrations can be designed, longitudinal exposure assessments in communities and households could enumerate the peak and duration of (di)isocyanate exposures; as stated, these values could then be contrasted against AD prevalence as well as symptom data from patients to evaluate whether exposure predicts disease severity and/or flares. If environmental detection remains limited, the TDI-haptenized albumin and anti-TDI IgE serum assays used in the diagnosis of diisocyanate-induced asthma (*59*) could be assessed for viability as biomarkers of diisocyanate exposure in AD.

Limitations in our methods for localizing AD rates include the provider-centric and aggregated nature of the database, which may be affected by access to care in the United States. However, our approach ensures provider-diagnosed AD as opposed to survey data

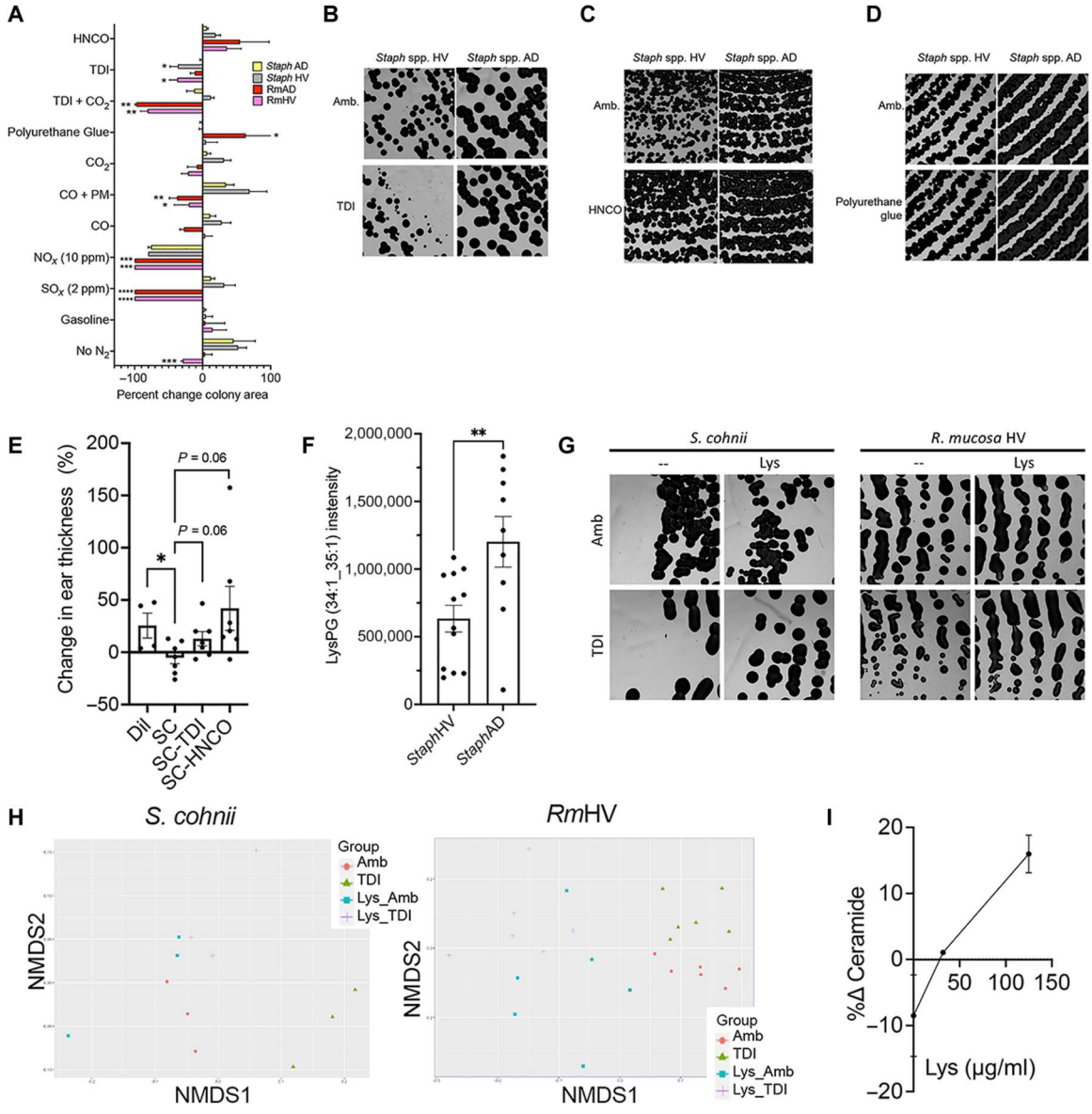

Fig. 8. TDI and HNCO disrupt beneficial pathways in *S. cohnii*. (**A**) Percent change in growth area for *Rm*HV1-3, *Rm*AD1-3, *Staph* HV1-3, and *Staph* AD1-3 as quantified from images shown in Figs. 1I, 2C, 4D, 5 (A, E, F, and I), and 8 (B to D and G). Significance is indicated versus *Staph* AD group. Impacts of NO_x on *Staph* taken from (*62*). (**B** to **D**) Representative image of *Staph* HV1-3 and *Staph* AD1-3 cultured with TDI (B), HNCO (C), or polyurethane-containing glue (D). (**E**) Change in mouse ear thickness in MC903 mouse model after treatment with *S. cohnii* grown under ambient conditions or with exposure to TDI or HNCO. (**F**) Intensity levels of LysPG identified by mass/charge ratio and collisional cross section for the three isolates of *Staph*HV and three isolates from *Staph*AD. (**G** and **H**) Representative images (G) and non-metric multidimensional scaling (NMDS) plots (H) for *S. cohnii* and *Rm*HV1 exposed to TDI with and without pretreatment with lysine (Lys) supplementation. (**I**) Change in total annotated ceramides with exposure to TDI versus ambient for *Rm*HV with and without Lys supplementation pretreatment. All images were taken at ×1.25 magnification. Data are representative of two or more independent experiments and are displayed as means ± SEM. *$P < 0.05$, **$P < 0.01$, and ***$P < 0.001$ as determined by ANOVA.

that may incorporate other forms of "eczema." Our pollution assessments are limited by the voluntary nature of TRI reporting, which could fail to detect unrecognized toxins and could not correct for factories that inaccurately report their pollution output. Our pollutant data sources could be expanded, and our modeling could also be improved via spatial and interaction considerations. Similarly, further investigation should assess the impact of the additional forms of diisocyanates or related compounds given the isocyanate use in our studies had overlapping but distinguishable impacts. For our clinical results, failure to reach statistical significance during active treatment, in part, was due to overperformance of the placebo arm compared to a priori powering expectations. This overperformance may have been caused by the addition of a vehicle effect stemming from protocol requirements for twice-daily moisturization using a ceramide-containing regimen optimized to avoid inducing dysbiosis (*16*) combined with potential prebiotics effects of the sucrose in the placebo formulation.

Aggregating the AD-associated pollutants (Fig. 3J) highlights the need to further evaluate potential synergy between environmental exposures associated with AD, most notably polychlorinated

biphenyls (Fig. 3E and fig. S4G) (*60*), CO_2 (fig. S9E), PM2.5 (*61*), NO_2 (fig. S4A) (*62*), and dysbiotic skin care products (*16*). Given the reported benefit of air purifiers in AD (*63*), our experiments demonstrating partial reduction of TDI levels using a common air purifier (fig. S6N) should be expanded to include additional types of filters and/or longer filtration times. These experiments will likely require improved detection equipment to assess which purification systems remove ambient (di)isocyanate well enough to protect commensal metabolism.

Although treatment fell short of the commercial goal of prescription licensure, given the highly favorable safety profile and evidence of exposome-responsive effects of *R. mucosa*, probiotic use could be considered while the needed environmental assessments and mitigation strategies are being elucidated. Additional consideration could be given to testing *R. mucosa* treatment as prevention against AD in high-risk infants; whether that risk is best defined by biologic markers such as epidermal water loss, family history, microbial markers, or environmental exposures remains to be elucidated. Furthermore, with the association of obesity with our AD regression models (Fig. 4, G and J) as well as the established propensity for the Western diet to promote atopy through dysbiosis (*34*), consideration should be given to exploring synergy between topical probiotics like *R. mucosa* and oral probiotics like select reported isolates of *Lactobacillus* and/or *Bifidobacterium* species (*64*). Furthermore, some of the pollutants we screened in our studies are more likely to be ingested and thus may be better screened for impacts using gut commensals instead of *R. mucosa*. This investigation would likely benefit from efficacy assessments with longer post-treatment washout times, avoidance of vehicle effect–inducing moisturizer regimens, targeted study site selection, and optimized strain selection focusing on the most potent *R. mucosa* isolate (*8*). To facilitate access for patients and researchers, we have thus renounced the patents on *R. mucosa* and deposited the isolate with the greatest efficacy in our models (*Rm*HV1) into both the National Institute of Standards and Technology (NIST) and American Type Culture Collection (ATCC) biobanks accessible to interested probiotic manufacturers or laboratories under the isolate name RSM2015.

MATERIALS AND METHODS

Clinical trial

Patients were enrolled under the Institutional Review Board–approved clinical trial NCT04504279 and FDA investigational new drug (IND) number 017303. All subjects provided written and verbal consent before participation in the study. Participants were enrolled and evaluated at one of 15 study sites: V. Laquer, Irvine, CA; M. Tepedino, Lake City, FL; M. Ling, Newman, GA; J. Browning, San Antonio, TX; F. Calcagno, Gresham, OR; S. Kempers, New Brighton, MN; C. Teller, Bellaire, TX; M. Landis, Corydon, MD; Z. Draelos, High Point, NC; S. Guenthner, Plainfield, GA; L. Green, Silver Spring, MD; S. Dhawan, Fremont, CA; C. Owens, Louisville, KY; S. Niazi, Lincoln, NE; and S. Lessin, Bryn Mawr, PA. Study sites were selected, and the study initiated before environmental assessments for dysbiosis was performed.

The multicenter, randomized, double-blind, placebo-controlled, parallel-group study enrolled 154 subjects (≥2 years of age) with mild to moderate AD involving at least 5% body surface area (BSA) and an EASI score of at least 5. Two weeks before enrollment, subjects were instructed to discontinue all TCS, topical calcineurin inhibitors (TCIs), and/or crisaborole. At enrollment, subjects were also told to begin a predetermined moisturizer regimen of either Cetaphil lotion, Aquaphor ointment, or Vanicream lotion/cream. Eligible subjects were then randomized 1:1 to treatment with FB-401 or matching placebo, topically applied, three times per week for 16 weeks. FB-401 consisted of a live therapeutic product consisting of equal colony-forming units (CFU) of three therapeutic strains of *R. mucosa* derived from the skin of three different healthy individuals. Participants were provided individual spray bottles with lyophilized *R. mucosa* with sucrose (treatment; FB-401) or sucrose alone (placebo).

Before administration, subjects (or parents/legal guardians) were to open the vial containing the lyophilized powder, reconstitute the powder with the sterile aqueous solution (yielding an FB-401 concentration of approximately 1×10^7 CFU/ml), and close the vial with the pump sprayer. After priming the sprayer, subjects (or parents/legal guardians) applied two sprays of FB-401 (totaling approximately 10^5 CFUs) to each AD-affected skin area. FB-401 was to be applied three times per week for 16 weeks, regardless of whether the area becomes clinically clear. The initial dose application on baseline/day 1 was applied in the clinic. Subjects or parents/legal guardians recorded each dose administered in a dosing diary. Subjects were evaluated for safety and efficacy every 4 weeks; active treatment lasted for 16 weeks, followed by a safety washout period of an additional 4 weeks in which the moisturizer regimen was to cease, but discontinuation of competing topical medications was to continue.

The inclusion criteria included the following: (i) male or female, ≥2 years of age; (ii) clinical diagnosis of AD as defined by Hanifin and Rajka criteria, which has been present for ≥3 months before the screening visit; (iii) IGA score of 2 (mild) or 3 (moderate) at screening and baseline/day 1 using the validated IGA scale for AD; (iv) EASI score ≥ 5 at the screening and baseline/day 1 visit; (v) ≥5% BSA of AD involvement at the screening and baseline/day 1 visit; (vi) table use of topical emollient (moisturizer) daily for at least 7 days before the baseline visit; (vii) contraception [sexually active female subjects of childbearing potential must agree to use adequate methods of contraception from the screening visit continuously until 30 days after stopping treatment with the investigational product; childbearing potential is defined for children as females who have begun menstruating and for adults as females who are not surgically sterile (hysterectomy and/or tubal ligation) or menopausal (no menstrual period for at least 12 months); adequate contraception methods include hormonal contraception or barrier method]; (viii) female subjects of childbearing potential must have negative serum pregnancy test results; (ix) subjects and parents/legal guardians (for children/adolescents) are willing and able to comply with all clinic visits and study-related procedures; (x) adult subjects ≥18 years of age have the ability to understand, agree to, and sign the informed consent form (ICF) before initiation of any protocol-related procedures; (xi) parents/legal guardians of subjects <18 years of age have the ability to understand, agree to, and sign the ICF, and subjects <18 years of age (who have the appropriate maturity and psychological ability) provide assent to participate in the study at the time of parent/legal guardian consent.

The exclusion criteria included the following (subjects meeting any of the criteria below will not be included in this study): (i) prior

participation in a study with FB-401; (ii) previous treatment [within 4 weeks before the baseline visit with any of the following: immunosuppressive or immunomodulating systemic drugs such as systemic corticosteroids, azathioprine, methotrexate, and cyclosporine and phototherapy or photochemotherapy for AD; within 1 week before the baseline visit with any of the following: TCS or TCIs; topical PDE4 inhibitor; emollients containing ceramides, hyaluronic acid, urea, or filaggrin degradation products; bleach baths; within 8 weeks or five half-lives (if known), whichever is longer, before the baseline visit with JAK inhibitors or other investigational drug; within 16 weeks or five half-lives, whichever is longer, before the baseline visit with dupilumab or other biologic agent]; (iii) regular use (twice per week or more) of tanning booth within 4 weeks of baseline visit; (iv) active infection (chronic or acute) requiring treatment with systemic antibiotics, antivirals, or antifungals within 2 weeks before the baseline visit; (v) superficial skin infection requiring topical treatment within 1 week of baseline visit; (vi) known or suspected history of immunosuppression, immunodeficiency, or neutropenia (<1000 cells/mm^3); (vii) history of human immunodeficiency virus (HIV) infection or positive HIV serology; (viii) history of hepatitis or positive serology; (ix) any clinically significant laboratory, in the investigator′s opinion, in screening laboratory evaluations; (x) skin disorders that would interfere with study assessments; (xi) severe concomitant illness that, in the investigator′s opinion, would adversely affect subject participation in the study, whether medical or psychological; (xii) pregnant or lactating females.

Primary end point was the percent change in EASI score from baseline to week 16 in the treatment versus placebo groups. Secondary end points included the proportion of subjects achieving EASI75, EASI90, proportion of subjects with an IGA score of 0 (clear) or 1 (almost clear) with a two-grade improvement, the percent change in pruritus numeric rating scale (NRS), proportion with an improvement in NRS of four or more points, change in BSA, percent change in sleep loss NRS score, and change in the patient-oriented eczema measure (POEM). Safety end points were adverse events and local tolerability. After trial completion, data were provided to NIH for verification and post hoc analysis of the population that completed the entire 20-week trial.

For the rate of IGA 0 to 1, EASI75, and EASI90, all enrollees with baseline values were included in the ITT analysis; if subjects withdrew or were lost to follow up, they were considered a treatment failure regardless of previous values. Percent change within a given participant was calculated by individual using corrected *t* test for each clinic visit week. The NIH license was restricted to prescription pharmaceutical development, and therefore, failure to achieve significance on the lone FDA metric for AD drug approval (ITT analysis of IGA 0 to 1) indicated that continuation to phase 3 was not economically justified. As such, a mutual agreement between NIH and Forte was reached that pursual of prescription approval would be abandoned; NIH was then allowed to perform post hoc analysis on the clinical data. For the completer population, only individuals with values for baseline and week 20 were considered unless they used steroids after week 12 of the trial; if steroids were used between weeks 12 to 20 (n = 2 for FB-401, 1 for placebo), the participant was excluded from analysis to avoid steroid confounding. NIH analysis used repeated-measures analysis of variance (rANOVA) rather than serial *t* tests. All NIH-based statistics were performed using Prism 9 (GraphPad, San Diego, CA).

Bacterial culture

Isolates of *R. mucosa* and *Staph* were selected as previously described (*8*, *16*, *49*) except for *S. cohnii*, which was purchased from ATCC (Manassas, VA), and isolates of *S. epidermidis* (13, 25, and 1457), which were cultured as previously described (*48*) and provided as a gift from M. Otto [National Institute of Allergy and Infectious Diseases (NIAID), Bethesda, MD]. All BioLog data were generated using an OmniLog per the manufacturer′s instructions (Hayward, CA). *Roseomonas* was grown in R2A broth (Teknova, Hollister, CA) or on R2A agar (Remel, San Diego, CA) at 32°C. In select experiments, the broth was supplemented with alanine, ATP, molybdenum, FeS, β-glucan from *Candida* spp., pyruvate, acetyl–coenzyme A, citrate, *cis*-aconitate, citrulline, NH_4Cl, lactic acid, Na nitrate, and NH_3, and all amino acids were each purchased from Sigma-Aldrich (St. Louis, MO). Nitrogen total was purchased from Merck (Germany). The medium limited in nitrogen or carbon was made by first making a stock of $MgSO_4•7H_2O$ (0.05 g/liter; Sigma-Aldrich), K_2HPO_4 (0.3 g/liter; Sigma-Aldrich), and Na pyruvate (0.3 g/liter; Sigma-Aldrich). Then, dextrose (2 g/liter) (Sigma-Aldrich) and soluble starch (0.5 g/liter) were added to generate nitrogen-free medium. Alternatively, amino acids (2.5 g/liter) (MP, no. 4400022) were added for carbohydrate-free medium, or both amino acids and dextrose (1.25 g/liter) were added for replete medium. All medium was sterilized using a SterileElite 24 autoclave (Fisher Science, Hampton, NH).

Recombinant human LL-37 was purchased from Novus Biologicals (Centennial, CO); in select experiments, LL-37 was then assayed using an enzyme-linked immunosorbent assay (ELISA) kit (Hycult Biotech, Wayne, PA) after 24 to 49 hours of growth to assess the remaining fraction of LL-37 versus input. In select experiments, cultures were placed into Hydroplate HP96U (PreSens, Regensburg, Germany) for pH monitoring per the manufacturer′s instructions using fluorescence signaling assessed on Cytation 5 running Gen5 (BioTek, Winooski, VT). Cytation 5 and Gen5 software were also used to take images at 1.25× of agar plates (BioTek). Area of coverage per image field of bacteria was calculated using ImageJ (Bethesda, MD). Acetate and lactate colorimetric kits (Sigma-Aldrich) were performed per the manufacturer′s instructions on lysed bacteria after 24 hours of culture on agar.

Probiotic formulation

Roseomonas capsules were made in by suspending an overnight culture in 10% sucrose, freezing to −70°C, and lyophilizing in a Labconco FreeZone 2.5 (Kansas City, MO) for 24 hours. Then, a heated shelf was activated (Labconco) and turned to 25°C using a 312C thermometer (PTC Instruments, Los Angeles, CA) for 1 hour. The sucrose/bacteria solution was removed and encapsulated in a capsule maker using 000-sized vegan capsules (All-In Capsules) along with 1% colloidal oatmeal (w/w) (Aveeno, Johnson & Johnson, New Brunswick, NJ). Capsules were stored at either 4°C, −20°C, or −70°C and assessed for change from staring colony concentration monthly. Viability against topical products was performed as previously described (*16*). Cooking oils were purchased from Mom′s Organic Market (Rockville, MD). Kiyamel was purchased online (kiyamel.com), as were Simple Sugars (simplesugarsskincare.com) and Rareglo (rareglo.com). All other indicated lotions, creams, and ointments were purchased from the Naval Exchange (Bethesda, MD) or Target department store (Rockville, MD).

Environmental exposures and assessments

Bacterial plates were placed in anaerobic chambers, either Torbal AJ-2, BBL Gaspak Jar, or a Torbal AJ-3 equipped with a digital Dwyer gauge (Grainger, Rockville, MD). $^{13}CO_2$ and SO_2 were purchased from Sigma-Aldrich. CO with PM was generated by lighting a match (Diamond long reach match, Barberton, OH) in the chamber, closing the lid and then opening the valves to allow O_2 to enter. Plates were placed in immediately after the match had extinguished, and the entire chamber was quickly sealed. A mixture of 80% $^{15}N_2$ and 20% O_2 was purchased from Sigma-Aldrich. Custom gas mixes were purchased from Roberts Oxygen (Rockville, MD). Gas detection tubes used included Gastec 112D, 110B, and 172L (Cairo, Egypt) and Draeger 100A (Houston, TX). Gas detection instruments were also connected to the culture chambers: AltAir 5X (MSA Safety, Cranberry Township, PA), GFG multigas detector G450 (Grainger), and H_2 Forensic detector (Rolling Hills Estates, CA).

4,4-MDI, 2,4-TDI, and toluene were purchased from Sigma-Aldrich. HNCO was purchased from A2B (San Diego, CA). Gasoline was collected in a sterile glass jar from the Navy Exchange Gas Station (Bethesda, MD). Diisocyanate-containing glue (clear Gorilla Glue) and polyurethane-based glue (Loctite PL Premium) were purchased from Strosniders Hardware (Kensington, MD). Diisocyanate-negative Onyx Green glue was purchased from Earth-Hero (Louisville, CO). Each was placed in the base of a glass petri dish (Pyrex Corning, #70165-100), while the base agar dish (plastic, Falcon, #35-1029) was inserted into it for tight fit.

For assessment of NO_2, R2A Agar Mix (Sigma-Aldrich) was placed in 100-mm polystyrene cell culture dishes (Corning, NY) and bacteria were plated (plating beads, Millipore, Burlington, MA). Bacteria on plates were exposed to 1 ppm of NO_2 for 48 hours in in vitro exposure chambers as previously described (*65*). NO_2 was provided at 20 liters/min, balanced with 5% CO_2, and at 88% relative humidity.

MDI/TDI measurements

Reported release levels for TDI and other diisocyanates were converted from pounds per year to milligrams per hour. In vitro measurements were performed by placing either 1 μl of 2,4-TDI (Sigma-Aldrich) or 1 g of either a diisocyanate-containing glue (clear Gorilla Glue) or polyurethane-based glue (Loctite PL Premium) in the base of a 1.8-liter mason jar (Ball, Westminster, CO). Two SafeAir MDI/TDI detector badges (Morphix, Virginia Beach, VA) were inserted and allowed to incubate at 23° to 37°C for 24 hours. Diisocyanate measurements were confirmed by use of SPM Flex monitor and SPM Flex Cassettes (Honeywell, Charlotte, NC). The monitor was placed immediately next to a glass agar plate with 1 μl of TDI or 1 g of the respective glues on a hotplate; minimum, maximum, and average readings were recorded over 60 min at 23°, 32°, and 37°C. Serial dilutions of TDI into toluene were performed to assess dose response for bacterial challenge as well as emission rate. Readouts were converted from ppb per hour to micrograms per cubic meter per hour using the standard equation μg/m^3 = [(ppb/hour)*12.187*(174.2; the molecular weight TDI)]/273.15 + temperature in Celsius.

Calculations correlating TDI concentration to resultant ppb were performed by assessing output from serially diluted 2,4-TDI beginning with a stock concentration of 1.2 mg/μl. One microliter was placed on a glass dish and heated to 32°C. Output over 15 min was measured by SPM Flex, and the average concentration was recorded for all values within the detection range (0.5 to 200 ppb). Log-log regression was performed to extrapolate the ppt values for dilutions with TDI aerosol outputs below 0.5 ppb.

For filtration experiments, 50 mg of 2,4-TDI (Sigma-Aldrich) was placed into 52-m^3 room at 21.8°C on a Pyrex glass petri dish lid (Corning, NY). Continuous monitoring was performed using the SPM Flex (Honeywell). After several hours, the TDI was placed on a hot plate set to 30°C. Prefiltration samples were collected by placing *S. epidermidis* or *R. mucosa* cultures on agar plates into a sealed Gaspak jar. The air was vacuumed out in a separate part of the building with no detectable TDI; control cultures were collected in this same part of the building, but the air was not removed. The seal was then released inside the room so that prefiltered air was pulled into the canister by vacuum pressure. Canisters were then sealed and placed at 32°C for 24 to 48 hours before assessment in downstream assays. After several hours, filtration was initiated using a Rabbit Air Minus2 air purifier with the "toxin absorber" insert reported to target volatile organic compounds (Pasadena, CA). TDI remained in the room with the purifier for several hours until the hot plate was turned off, but the TDI remained in the room. Postfiltration samples were collected in an identical fashion to prefiltration samples.

MALDI assessment of bacteria

Bacterial pellets from broth cultures or loops (Fisherbrand, #22-363-606) were placed into 2,5-dihydroxybenzoic acid (DHB) (20 mg/ml; #149357-10G, Sigma-Aldrich) matrix solution in 70% methanol (Sigma-Aldrich) and 0.1% trifluoroacetic acid (TFA; Sigma-Aldrich). Samples were then plated on spot plates (Bruker, Billerica, MA). Plates were cleaned between uses in 100% methanol in E+ Easy Elmasonic (Elma, Quebec, Canada). All MALDI data were collected using timsControl (Bruker). MS settings: scan range, 20 to 2500 mass/charge ratio (m/z) on negative MS scan mode. TIMS settings: 1/K0, 0.8 to 1.8 V*s/cm^2. Ramp time, 73 ms; Accu time, 20 ms; duty cycle, −27.4%; and ramp rate, 12.64 Hz. Annotations were performed on Metaboscape 2021b, as were *t* tests for comparison between indicated conditions. In select experiments, annotations were searched for "Cer" and total intensity for ceramide containing annotations was exported and summed.

Keratinocyte cultures

Primary neonatal human keratinocytes (ATCC) were seeded in a 24-well cell culture plate that was previously coated with solution of human fibronectin (10 μg/ml; Millipore Sigma) in sterile phosphate-buffered saline (PBS) at a density of 1.5×10^5 cells per well (3.75×10^5 cells/ml, added in 400-μl volume) in Defined Keratinocyte Serum Free Medium (Gibco). Cells adhered to the plate after 2 hours. *S. epidermidis* isolates were scraped off agar plates, suspended in PBS at OD_{600} (optical density at 600 nm) = 1.2, adjusted to 3.75×10^5 CFU/ml in keratinocyte medium, and added to wells with or without cells in 400-μl volume. Wells with cells were infected at a multiplicity of infection of 1. After overnight incubation, supernatants were collected by centrifugation at 15,000 rpm for 7 min. Two hundred microliters of 100% methanol was added to the dry wells to lyse the keratinocytes (KC). One hundred microliters of the lysed KC was added to the supernatant and diluted 1:10 in 20 mg/ml of DHB matrix solution in 70% methanol and 0.1% TFA as above. MALDI analysis for ceramides and pathways was then performed in an identical manner as for the bacteria.

Mouse model

All murine experiments were done in compliance with the guidelines of the NIAID Institutional Animal Care and Use Committee. MC903 model of AD using *Roseomonas* was performed as previously described using C57BL/6 wild-type mice aged 6 to 10 weeks purchased from The Jackson Laboratory. Briefly, from days −8 to 0, mice were treated with 10 μl of MC903 diluted in ethanol applied to each ear. On day 0, ear thickness was measured, and mice were topically treated with 10 μl of 1×10^6 *R. mucosa* or 1×10^5 *S. cohnii*. On day 6, all mice were euthanized, and ears were measured and collected. After collecting the mouse ear in Tissue-Tek Cryomold (Sakura, #4557) containing optimal cutting temperature (OCT) compound clear for frozen tissue (Fisher Scientific, #4585), tissue was placed on OCT and extra OCT was layered on top of tissue followed by placing cryomold in liquid N_2 tank for 2 hours and transferred to −70°C freezer until samples were sectioned and placed on IntelliSlides (#1868957, Bruker) and stored at −70°C until mounted on IntelliSlides (Bruker) by HistoServ Inc. (Germantown, MD). Slides were placed in desiccator and, after drying, imaged with tissue scout (Bruker). Slides were placed in the TM sprayer from HTX Technologies LLC, and DHB (20 mg/ml; #149357-10G, Sigma-Aldrich) matrix solution was prepared in 100% acetone and 0.1% TFA (Sigma-Aldrich, #302031). The following method was used to spray all the slides: Nozzle temperature was at 50°C, plate rate was set at 0.100 ml/min, Z arm velocity was 1200, number of passes was 14, moving pattern was CC, and track spacing was kept at 2. After spraying the slides with matrix solution, slides were loaded in the slide holder from Bruker and run in timsTOF flex (Bruker). For MALDI imaging, all the slides were imaged for ion polarity mode positive. Tissue was scanned for both MS and TIMS setting at the resolution of 20 μm. MS settings: scan range of 20 to 2500 m/z on a positive MS scan mode. TIMS settings: 1/K0, 0.8 to 1.89 V*s/cm^2. Ramp time, 200 ms; Accu time, 20 ms; duty cycle, −10%; and ramp rate, 4.85 Hz.

^{15}N and ^{13}C flux metabolic analysis

Flux analysis was performed commercially by Phenoswitch (Sherbrooke, QC Canada). For ^{13}C, 65 μl of cold extraction buffer [2:2:1 acetonitrile (ACN):MeOH:H_2O] containing heavy-labeled amino acids as internal standard was added on the frozen pellets. Each sample was then vortexed for 5 s and incubated on ice for 20 min. After centrifugation, supernatant was placed in a new tube and 35 μl of extraction buffer was readded to the pellet. Another round of vortex and incubation was performed, and the resulting supernatant was combined with the first extraction. This mixture was split in two fractions [66 μl for reverse phase (RP) and 33 for hydrophilic interaction liquid chromatography (HILIC)] and dried under nitrogen gas. The first half of the extract was reconstituted in 20 μl of water + 0.1% fatty acid (FA) and the other half in 20 μl of ACN + 0.1% FA. The fraction that was reconstituted in water was analyzed using reversed-phase chromatography in both positive and negative modes. The fraction that was reconstituted in ACN was analyzed using HILIC chromatography in a positive mode.

Acquisition was performed with ABSciex TripleTOF 5600 (ABSciex, Foster City, CA, USA) equipped with an electrospray interface with a 50-μm inside diameter capillary and coupled to a Nexera UHPLC. Analyst TF 1.7 software was used to control the instrument and for data processing and acquisition. Acquisition was performed in information-dependent acquisition (IDA) mode for both the positive and negative ionization modes. For the positive ionization, the source voltage was set to 5.5 kV and maintained at 220°C, curtain gas was set at 30 psi, gas one was set at 30 psi, and gas two was set at 40 psi. For the negative ionization, the source voltage was set to 4.5 kV and maintained at 220°C, curtain gas was set at 30 psi, gas one was set at 30 psi, and gas two was set at 40 psi. For the reversed phase, separation was performed on a reversed-phase Kinetex EVO, column 2.1 mm inside diameter, 2.6 μm particles, 100 mm long (Phenomenex), which was maintained at 50°C. For HILIC, separation was performed on a reversed-phase Luna Omega Sugar, column 2.1 mm inside diameter, 2.6 μm particles, 100 mm long (Phenomenex), which was maintained at 50°C. For the positive RP and HILIC 15-min liquid chromatography (LC) gradient, the mobile phase consisted of the following solvent A (H_2O + 0.1% FA) and solvent B (ACN + 0.1% FA) at a flow rate of 400 μl/min. For the negative mode, the mobile phase consisted of the following: solvent A (H_2O + 2 mM NH_4 acetate) and solvent B [ACN:MeOH (90:10) 2 mM NH_4 acetate] at a flow rate of 400 μl/min. Data were analyzed using MS-Dial. Identification for the metabolites was done using a curated version of the Massbank ion libraries. All the data were then concatenated in the data report. The calculated tab contains all the concatenated data.

For 15N, 400 μl of ice-cold methanol containing butylated hydroxytoluene (BHT) (50 mg/ml) and internal standard and 800 μl of ice-cold chloroform were added to the cell pellets. Samples were incubated on ice and vortexed a few times. Three hundred microliters of ice-cold water was added to each sample, and the phases were separated by centrifugation. The bottom phase (organic) was transferred in another tube, and 400 μl of 1:2 (methanol:chloroform) was added to the remaining aqueous phase. Samples were vortexed once more and centrifuged. The bottom phase was pooled with the first extraction and dried under nitrogen. Samples were reconstituted in 40 μl of 90:10 isopropanol:ACN + 10 mM NH_4 formate + 0.1% FA and analyzed by LC-MS/MS. Acquisition was performed with ABSciex TripleTOF 5600 (ABSciex, Foster City, CA, USA) equipped with an electrospray interface with a 50-μm iD capillary and coupled to a Nexera UHPLC. Analyst TF 1.7 software was used to control the instrument and for data processing and acquisition. Acquisition was performed in the IDA mode for both the positive and negative ionization modes. For the positive ionization, the source voltage was set to 5.5 kV and maintained at 220°C, curtain gas was set at 30 psi, gas one was set at 30 psi, and gas two was set at 40 psi. For the negative ionization, the source voltage was set to 4.5 kV and maintained at 220°C, curtain gas was set at 30 psi, gas one was set at 30 psi, and gas two was set at 40 psi. For the positive and negative modes, the mobile phase consisted of the following: solvent A (60:40 ACN:H_2O + 10 mM NH_4 formate + 0.1% FA) and solvent B (90:10 isopropanol:ACN + 10 mM NH_4 formate + 0.1% FA at a flow rate of 400 μl/min). Data were analyzed using MS-Dial. Identification of the metabolites was done using a curated version of the Massbank ion libraries. All the data were then concatenated in the data report. The calculated tab contains all the concatenated data.

Raw data were provided and analyzed further for pathways by taking metabolites ranked by P values for differentiation between conditions. These were analyzed by MetaboAnalyst under default settings using human KEGG (Kyoto Encyclopedia of Genes and Genomes), murine KEGG, or *Escherichia coli* KEGG pathways where appropriate.

For additional analysis, full bucket tables were exported from Metaboscape 2021b for further statistical data analysis in R. Nonmetric dimensional scaling was carried out in R using the vegan package. To find out the statistical significance between the metabolite′s concentration between the groups, analysis of similarities (ANOSIM) was used.

For heatmap generation, *P* values (false discovery rate) based on ANOVA or *t* test between all the combination groups were also calculated in Metaboscape 2021b, and table was exported in R further to plot the heatmap between the top 50 most significantly different metabolites between the comparisons. Pheatmap library was used to plot the heatmap in R. After peak intensity table was imported, the uploaded data were log-transformed, and normalization was done by mean subtraction. Other parameters that were set included use of the correlation-based clustering of the columns. To simplify the visualization of the abundances of the metabolites across the treatments, the top 50 metabolites ranked by ANOVA or *t* test are shown.

Nation-level gas analysis

AD rates by nation were taken from citation (*66*, *67*). MDI and TDI production levels by year were identified from CDC (*68*), Statista (*69*, *70*), and Markit (*71*). National production of TDI was taken from (*72*).

Gas chromatography

The gas chromatography (GC) measurements were performed on an Agilent 6890N system coupled with a JEOL high-resolution magnetic sector mass spectrometer (JMS-700 MStation) with the electron ionization (EI) ion source (70 eV). The mass spectrometer was operated in the mode of high scan speed and low resolution (1000) with the mass range from 2 to 200 Da. A silica capillary column (Agilent DB-5, 60 m length, 250 μm inside diameter) was used with helium (at 1 ml/min) as the carrier gas. Analysis was performed as follows: 250 μl of head-space volatile organic compounds (VOC) were injected into the GC port. Analysis was performed using the splitless mode. The inlet temperature was 200°C, and the column temperature was programmed from 40°C at 4.0 min, increased to 200°C at the rate of 40°C/min, and then held at 200°C for another 2.0 min.

Mapping AD versus pollution

Data on pollution were derived from EPA′s TRI from 2012 to 2019. TRI represents data on about 500 compounds each year with known or suspected deleterious effects on human or environmental health. Industries are required by law to report their releases to TRI if their facility emits above a certain threshold. These data are reported by the type of chemical released, the quantity released in pounds, the latitude and longitude of each releasing facility, and the method of release (into water, via controlled release via stack, or fugitive release to the air). Pollution was analyzed in the same year not only as disease but also as a summation over the 5 years prior plus the year under analysis. Missing data on latitudes and longitudes were imputed by searching facility addresses on Google Maps. SaTScan (Harvard Medical School, Boston, MA) was used to derive cluster analysis, and Tableau public (Washington, DC) was used for mapping visualization.

The Definitive Health database contains 1.2 billion diagnostic billing codes per year from 2017 to 2019 across 20,000 zip codes in the United States, including Hawaii, Alaska, and the U.S. territories. The total number of billing codes for any diagnoses and the number of billing codes for AD specifically (L20.9) were collated by zip code. However, the data can be subsetted by specific specialties. For each disease tested, a unique subset of specialists was chosen. For AD, family practice, general practice, pediatrics, allergy/immunology, dermatology, and other generalist practices were selected. For the pediatric-only analysis, only pediatrics, adolescent medicine, pediatric allergy/immunology, and other pediatric specialties were selected. To account for the relative abundance of specialists, the proportion of total diagnoses from any given specialty in a zip code was divided by the total number of diagnoses in that zip code to create additional specialist variables.

Demographic data were extracted from the 2019 American Community Survey from the U.S. Census. For each zip code in the Definitive Healthcare database, population density was based on aggregating zip codes with centroids in a 30-mile radius around the zip code of interest. The percentage of the population under the age of 5 in that same 30-mile radius was also calculated. Missing data for the U.S. territories were researched separately and imputed manually. Data on whether a zip code was urban, a large rural town, or a small rural town were derived from the University of Washington Rural Health Research Center′s Rural Urban Commuting Areas, using categorization scheme B. The Area Deprivation Index for each census tract in 2019 was taken from the University of Wisconsin′s Neighborhood Atlas. These census tracts were converted to zip codes using cross-walk files from the U.S. Department of Housing and Urban Development. Missing deprivation data were imputed with the mean. Data on the obesity covariate [International classification of disease (ICD) codes starting with E66] in each zip code were derived from the Definitive Health database and were constructed as the average number of obesity patients per provider. Missing obesity data were imputed with a Poisson regression based on the deprivation index and the two demographic variables. The number of privately owned pools per capita was derived from Data Masters and aggregated on the county level. These counties were converted to zip codes such that zip codes on the border between multiple counties were taken as the average of those counties. Missing pool ownership data were imputed with the mean.

For each of the 20,000 zip codes in the Definitive Healthcare database, we define a 30-mile catchment area around the zip code centroid. For all facilities within the catchment area, the total amount of each pollutant is summed. If there are no facilities releasing a particular pollutant in the catchment area, that zip code is assigned zero for that pollutant. Because the zip code represents the location of the outpatient provider, rather than the residence of the patient, a Gaussian distribution is defined to weight the relative importance of facilities based on the distance from the zip code center. The center of the distribution is the centroid of the zip code where the provider is located, and the SD is 10.7785 miles, which is derived from the assumption that the mean distance between a patient and their provider is 8.6 miles (*73*).

Regression with an L1 regularization term (lasso regression) was used for feature selection via the "glmnet" package (*74*). Linear regression included weights equal to the total diagnostic billings per zip code, and Poisson regression included an offset equal to the total diagnostic billings per zip code. The lambda was selected by 10-fold cross-validation to minimize Poisson deviance in the case of Poisson regression and mean-squared error in the case of linear

regression. All features were standardized, and those with zero variance were removed before lasso regression. The rural, town, urban categorical variable was converted into three dummy variables.

Additional variable importance metrics were performed via Akaike information criterion (AIC) forward and backward stepwise selection via the "MASS" package. The random forest was accomplished via the "ranger" package (*75*) so that weights could be assigned to each zip code, and the "pdp" package (*76*) was used to create partial dependence plots. Random forest was grown with 1000 trees with sampling of one-third the number of variables at each spit and with importance set to "impurity," which measures variance of the response. Principal components analysis was used to visualize separation between three quantiles of AD burden based on pollution variables.

Supplementary Materials

This PDF file includes:

Figs. S1 to S10

View/request a protocol for this paper from *Bio-protocol*.

REFERENCES AND NOTES

1. A. Paller, J. C. Jaworski, E. L. Simpson, M. Boguniewicz, J. J. Russell, J. K. Block, S. Tofte, J. D. Dunn, S. R. Feldman, A. R. Clark, G. Schwartz, L. F. Eichenfield, Major comorbidities of atopic dermatitis: Beyond allergic disorders. *Am. J. Clin. Dermatol.* **19**, 821–838 (2018).
2. H. A. Hadi, A. I. Tarmizi, K. A. Khalid, M. Gajdács, A. Aslam, S. Jamshed, The epidemiology and global burden of atopic dermatitis: A narrative review. *Life (Basel)* **11**, 936 (2021).
3. C. S. Benn, M. Melbye, J. Wohlfahrt, B. Björkstén, P. Aaby, Cohort study of sibling effect, infectious diseases, and risk of atopic dermatitis during first 18 months of life. *BMJ* **328**, 1223 (2004).
4. W. Karmaus, C. Botezan, Does a higher number of siblings protect against the development of allergy and asthma? A review. *J. Epidemiol. Commun. Health* **56**, 209–217 (2002).
5. Y. Wang, K. J. Allen, N. H. A. Suaini, R. L. Peters, A.-L. Ponsonby, J. J. Koplin, Asian children living in Australia have a different profile of allergy and anaphylaxis than Australian-born children: A state-wide survey. *Clin. Exp. Allergy* **48**, 1317–1324 (2018).
6. E. H. Tham, E. X. L. Loo, Y. Zhu, L. P.-C. Shek, Effects of migration on allergic diseases. *Int. Arch. Allergy Immunol.* **178**, 128–140 (2019).
7. J. A. Odhiambo, H. C. Williams, T. O. Clayton, C. F. Robertson, M. I. Asher; ISAAC Phase Three Study Group, Global variations in prevalence of eczema symptoms in children from ISAAC Phase Three. *J. Allergy Clin. Immunol.* **124**, 1251–1258.e23 (2009).
8. I. A. Myles, C. R. Castillo, K. D. Barbian, K. Kanakabandi, K. Virtaneva, E. Fitzmeyer, M. Paneru, F. Otaizo-Carrasquero, T. G. Myers, T. E. Markowitz, I. N. Moore, X. Liu, M. Ferrer, Y. Sakamachi, S. Garantziotis, M. Swamydas, M. S. Lionakis, E. D. Anderson, N. J. Earland, S. Ganesan, A. A. Sun, J. R. E. Bergerson, R. A. Silverman, M. Petersen, C. A. Martens, S. K. Datta, Therapeutic responses to *Roseomonas mucosa* in atopic dermatitis may involve lipid-mediated TNF-related epithelial repair. *Sci. Transl. Med.* **12**, eaaz8631 (2020).
9. I. A. Myles, N. J. Earland, E. D. Anderson, I. N. Moore, M. D. Kieh, K. W. Williams, A. Saleem, N. M. Fontecilla, P. A. Welch, D. A. Darnell, L. A. Barnhart, A. A. Sun, G. Uzel, S. K. Datta, First-in-human topical microbiome transplantation with *Roseomonas mucosa* for atopic dermatitis. *JCI Insight* **3**, e120608 (2018).
10. L. Li, Z. Han, X. Niu, G. Zhang, Y. Jia, S. Zhang, C. He, Probiotic supplementation for prevention of atopic dermatitis in infants and children: A systematic review and meta-analysis. *Am. J. Clin. Dermatol.* **20**, 367–377 (2019).
11. T. Nakatsuji, T. R. Hata, Y. Tong, J. Y. Cheng, F. Shafiq, A. M. Butcher, S. S. Salem, S. L. Brinton, A. K. Rudman Spergel, K. Johnson, B. Jepson, A. Calatroni, G. David, M. Ramirez-Gama, P. Taylor, D. Y. M. Leung, R. L. Gallo, Development of a human skin commensal microbe for bacteriotherapy of atopic dermatitis and use in a phase 1 randomized clinical trial. *Nat. Med.* **27**, 700–709 (2021).
12. J. Mashiah, T. Karady, N. Fliss-Isakov, E. Sprecher, D. Slodownik, O. Artzi, L. Samuelov, E. Ellenbogen, A. Godneva, E. Segal, N. Maharshak, Clinical efficacy of fecal microbial transplantation treatment in adults with moderate-to-severe atopic dermatitis. *Immun. Inflamm. Dis.* **10**, e570 (2021).
13. T. Kobayashi, M. Glatz, K. Horiuchi, H. Kawasaki, H. Akiyama, D. H. Kaplan, H. H. Kong, M. Amagai, K. Nagao, Dysbiosis and *Staphylococcus aureus* colonization drives inflammation in atopic dermatitis. *Immunity* **42**, 756–766 (2015).
14. I. A. Myles, K. W. Williams, J. D. Reckhow, M. L. Jammeh, N. B. Pincus, I. Sastalla, D. Saleem, K. D. Stone, S. K. Datta, Transplantation of human skin microbiota in models of atopic dermatitis. *JCI Insight* **1**, e86955 (2016).
15. I. A. Myles, J. D. Reckhow, K. W. Williams, I. Sastalla, K. M. Frank, S. K. Datta, A method for culturing Gram-negative skin microbiota. *BMC Microbiol.* **16**, 60 (2016).
16. C. R. Castillo, M. E. Alishahedani, P. Gough, P. P. Chaudhary, M. Yadav, J. Matriz, I. A. Myles, Assessing the effects of common topical exposures on skin bacteria associated with atopic dermatitis. *Skin Health Dis.* **1**, e41 (2021).
17. J. van Smeden, J. A. Bouwstra, Stratum corneum lipids: Their role for the skin barrier function in healthy subjects and atopic dermatitis patients. *Curr. Probl. Dermatol.* **49**, 8–26 (2016).
18. A. Shea, M. Wolcott, S. Daefler, D. A. Rozak, Biolog phenotype microarrays. *Methods Mol. Biol.* **881**, 331–373 (2012).
19. Y. Lai, A. L. Cogen, K. A. Radek, H. J. Park, D. T. Mac Leod, A. Leichtle, A. F. Ryan, A. D. Nardo, R. L. Gallo, Activation of TLR2 by a small molecule produced by *Staphylococcus epidermidis* increases antimicrobial defense against bacterial skin infections. *J. Invest. Dermatol.* **130**, 2211–2221 (2010).
20. H. D. Graven, R. F. Keeling, S. C. Piper, P. K. Patra, B. B. Stephens, S. C. Wofsy, L. R. Welp, C. Sweeney, P. P. Tans, J. J. Kelley, B. C. Daube, E. A. Kort, G. W. Santoni, J. D. Bent, Enhanced seasonal exchange of CO_2 by northern ecosystems since 1960. *Science* **341**, 1085–1089 (2013).
21. A. B. Fleischer Jr., Atopic dermatitis: The relationship to temperature and seasonality in the United States. *Int. J. Dermatol.* **58**, 465–471 (2019).
22. V. Sojo, B. Herschy, A. Whicher, E. Camprubi, N. Lane, The origin of life in alkaline hydrothermal vents. *Astrobiology* **16**, 181–197 (2016).
23. E. Proksch, pH in nature, humans and skin. *J. Dermatol.* **45**, 1044–1052 (2018).
24. K. Ahn, The role of air pollutants in atopic dermatitis. *J. Allergy Clin. Immunol.* **134**, 993–999 (2014).
25. B. Tury, D. Pemberton, R. E. Bailey, Fate and potential environmental effects of methylenediphenyl diisocyanate and toluene diisocyanate released into the atmosphere. *J. Air Waste Manag. Assoc.* **53**, 61–66 (2003).
26. S. M. Langan, P. Silcocks, H. C. Williams, What causes flares of eczema in children? *Br. J. Dermatol.* **161**, 640–646 (2009).
27. J. H. Lee, J. Suh, E. H. Kim, J. B. Cho, H. Y. Park, J. Kim, K. Ahn, H. K. Cheong, S.-I. Lee, Surveillance of home environment in children with atopic dermatitis: A questionnaire survey. *Asia Pac. Allergy* **2**, 59–66 (2012).
28. S.-J. Yi, C. Shon, K.-D. Min, H.-C. Kim, J.-H. Leem, H.-J. Kwon, S. Hong, K. S. Kim, S.-Y. Kim, Association between exposure to traffic-related air pollution and prevalence of allergic diseases in children, Seoul, Korea. *Biomed. Res. Int.* **2017**, 4216107 (2017).
29. C. Pénard-Morand, C. Raherison, D. Charpin, C. Kopferschmitt, F. Lavaud, D. Caillaud, I. Annesi-Maesano, Long-term exposure to close-proximity air pollution and asthma and allergies in urban children. *Eur. Respir. J.* **36**, 33–40 (2010).
30. P. Kathuria, J. I. Silverberg, Association of pollution and climate with atopic eczema in US children. *Pediatr. Allergy Immunol.* **27**, 478–485 (2016).
31. Y. Miyake, K. Tanaka, H. Fujiwara, Y. Mitani, H. Ikemi, S. Sasaki, Y. Ohya, Y. Hirota, Residential proximity to main roads during pregnancy and the risk of allergic disorders in Japanese infants: The Osaka Maternal and Child Health Study. *Pediatr. Allergy Immunol.* **21**, 22–28 (2010).
32. M. Mubanga, C. Lundholm, B. M. D'Onofrio, M. Stratmann, A. Hedman, C. Almqvist, Association of early life exposure to antibiotics with risk of atopic dermatitis in Sweden. *JAMA Netw. Open* **4**, e215245 (2021).
33. EPA, in *Greenhouse Gas Emissions* (EPA, 2021).
34. J. Tan, C. McKenzie, P. J. Vuillermin, G. Goverse, C. G. Vinuesa, R. E. Mebius, L. Macia, C. R. Mackay, Dietary fiber and bacterial SCFA enhance oral tolerance and protect against food allergy through diverse cellular pathways. *Cell Rep.* **15**, 2809–2824 (2016).
35. D. Johnson, V. Letchumanan, S. Thurairajasingam, L.-H. Lee, A revolutionizing approach to autism spectrum disorder using the microbiome. *Nutrients* **12**, 1983 (2020).
36. B. Golofast, K. Vales, The connection between microbiome and schizophrenia. *Neurosci. Biobehav. Rev.* **108**, 712–731 (2020).
37. X. Liang, C. Ou, J. Zhuang, J. Li, F. Zhang, Y. Zhong, Y. Chen, Interplay between skin microbiota dysbiosis and the host immune system in psoriasis: Potential pathogenesis. *Front. Immunol.* **12**, 764384 (2021).
38. Toluene diisocyanates. *IARC Monogr. Eval. Carcinog. Risks Hum.* **71**, 865–879 (1999).
39. A. V. Wisnewski, J. Liu, C. A. Redlich, Antigenic changes in human albumin caused by reactivity with the occupational allergen diphenylmethane diisocyanate. *Anal. Biochem.* **400**, 251–258 (2010).
40. P. Mydel, Z. Wang, M. Brisslert, A. Hellvard, L. E. Dahlberg, S. L. Hazen, M. Bokarewa, Carbamylation-dependent activation of T cells: A novel mechanism in the pathogenesis of autoimmune arthritis. *J. Immunol.* **184**, 6882–6890 (2010).

41. R. P. Fadadu, B. Grimes, N. P. Jewell, J. Vargo, A. T. Young, K. Abuabara, J. R. Balmes, M. L. Wei, Association of wildfire air pollution and health care use for atopic dermatitis and itch. *JAMA Dermatol.* **157**, 658–666 (2021).
42. O. Herbarth, G. J. Fritz, M. Rehwagen, M. Richter, S. Röder, U. Schlink, Association between indoor renovation activities and eczema in early childhood. *Int. J. Hyg. Environ. Health* **209**, 241–247 (2006).
43. J. M. Roberts, P. R. Veres, A. K. Cochran, C. Warneke, I. R. Burling, R. J. Yokelson, B. Lerner, J. B. Gilman, W. C. Kuster, R. Fall, J. de Gouw, Isocyanic acid in the atmosphere and its possible link to smoke-related health effects. *Proc. Natl. Acad. Sci. U.S.A.* **108**, 8966–8971 (2011).
44. L. Bengtstrom, M. Salden, A. A. Stec, The role of isocyanates in fire toxicity. *Fire Sci. Rev.* **5**, 4 (2016).
45. M. D. Leslie, M. Ridoli, J. G. Murphy, N. Borduas-Dedekind, Isocyanic acid (HNCO) and its fate in the atmosphere: A review. *Environ. Sci. Process. Impacts* **21**, 793–808 (2019).
46. K. K. McCleary, K. Barta, L. Butler, K. Capozza, S. Eftekhari, K. Kelley, W.S. Begolka, K. Tullos, and T. Winders. The More Than Skin Deep "Voice of the Patient" Report (2020). Accessed May 2022, http://www.morethanskindeep-eczema.org/uploads/1/2/5/3/125377765/mtsd_report_-_digital_file_1.pdf.
47. Y. Ito, T. Sasaki, Y. Li, T. Tanoue, Y. Sugiura, A. N. Skelly, W. Suda, Y. Kawashima, N. Okahashi, E. Watanabe, H. Horikawa, A. Shiohama, R. Kurokawa, E. Kawakami, H. Iseki, H. Kawasaki, Y. Iwakura, A. Shiota, L. Yu, J. Hisatsune, H. Koseki, M. Sugai, M. Arita, O. Ohara, T. Matsui, M. Suematsu, M. Hattori, K. Atarashi, M. Amagai, K. Honda, *Staphylococcus cohnii* is a potentially biotherapeutic skin commensal alleviating skin inflammation. *Cell Rep.* **35**, 109052 (2021).
48. Y. Zheng, R. L. Hunt, A. E. Villaruz, E. L. Fisher, R. Liu, Q. Liu, G. Y. C. Cheung, M. Li, M. Otto, Commensal *Staphylococcus epidermidis* contributes to skin barrier homeostasis by generating protective ceramides. *Cell Host Microbe* **30**, 301–313.e9 (2022).
49. I. A. Myles, I. N. Moore, C. R. Castillo, S. K. Datta, Differing virulence of healthy skin commensals in mouse models of infection. *Front. Cell. Infect. Microbiol.* **8**, 451 (2018).
50. Y. Oku, K. Kurokawa, N. Ichihashi, K. Sekimizu, Characterization of the *Staphylococcus aureus mprF* gene, involved in lysinylation of phosphatidylglycerol. *Microbiology (Reading)* **150**, 45–51 (2004).
51. S. Delanghe, J. R. Delanghe, R. Speeckaert, W. Van Biesen, M. M. Speeckaert, Mechanisms and consequences of carbamoylation. *Nat. Rev. Nephrol.* **13**, 580–593 (2017).
52. B. C. Martel, P. Lovato, W. Baumer, T. Olivry, Translational animal models of atopic dermatitis for preclinical studies. *Yale J. Biol. Med.* **90**, 389–402 (2017).
53. D. Hayes-Green, B. P. Love, *The Groundwater Approach: Building a Practical Understanding of Structural Racism* (The Racial Equity Institute, 2018).
54. S. A. Smits, J. Leach, E. D. Sonnenburg, C. G. Gonzalez, J. S. Lichtman, G. Reid, R. Knight, A. Manjurano, J. Changalucha, J. E. Elias, M. G. Dominguez-Bello, J. L. Sonnenburg, Seasonal cycling in the gut microbiome of the Hadza hunter-gatherers of Tanzania. *Science* **357**, 802–806 (2017).
55. G. I. Perez Perez, Z. Gao, R. Jourdain, J. Ramirez, F. Gany, C. Clavaud, J. Demaude, L. Breton, M. J. Blaser, Body site is a more determinant factor than human population diversity in the healthy skin microbiome. *PLOS ONE* **11**, e0151990 (2016).
56. T. Sakai, N. Herrmann, L. Maintz, T. J. Nümm, T. Welchowski, R. A. Claus, M. H. Gräler, T. Bieber, Altered serum phospholipids in atopic dermatitis and association with clinical status. *JID Innov.* **2**, 100092 (2021).
57. S. Mihara, T. Shibamoto, The role of flavor and fragrance chemicals in TRPA1 (transient receptor potential cation channel, member A1) activity associated with allergies. *Allergy Asthma Clin. Immunol.* **11**, 11 (2015).
58. F. M. S. Badloe, S. De Vriese, K. Coolens, C. B. Schmidt-Weber, J. Ring, J. Gutermuth, I. K. Krohn, IgE autoantibodies and autoreactive T cells and their role in children and adults with atopic dermatitis. *Clin. Transl. Allergy* **10**, 34 (2020).
59. H. S. Park, S. K. Lee, Y. M. Lee, S. S. Kim, D. H. Nahm, Longitudinal study of specific antibodies to toluene diisocyanate (TDI)-human serum albumin (HSA) conjugate in patients with TDI-induced asthma. *Korean J. Intern. Med.* **17**, 249–251 (2002).
60. M. Parker-Lalomio, K. McCann, J. Piorkowski, S. Freels, V. W. Persky, Prenatal exposure to polychlorinated biphenyls and asthma, eczema/hay fever, and frequent ear infections. *J. Asthma* **55**, 1105–1115 (2018).
61. B. E. Kim, J. Kim, E. Goleva, E. Berdyshev, J. Lee, K. A. Vang, U. H. Lee, S. Y. Han, S. Leung, C. F. Hall, N.-R. Kim, I. Bronova, E. J. Lee, H.-R. Yang, D. Y. Leung, K. Ahn, Particulate matter causes skin barrier dysfunction. *JCI Insight* **6**, e145185 (2021).
62. X. Janvier, S. Alexandre, A. M. Boukerb, D. Souak, O. Maillot, M. Barreau, F. Gouriou, C. Grillon, M. G. J. Feuilloley, A. Groboillot, Deleterious effects of an air pollutant (NO_2) on a selection of commensal skin bacterial strains, potential contributor to dysbiosis? *Front. Microbiol.* **11**, 591839 (2020).
63. M.-T. Lee, C.-C. Wu, C.-Y. Ou, J.-C. Chang, C.-A. Liu, C.-L. Wang, H. Chuang, H.-C. Kuo, T.-Y. Hsu, C.-P. Chen, K. D. Yang, A prospective birth cohort study of different risk factors for development of allergic diseases in offspring of non-atopic parents. *Oncotarget* **8**, 10858–10870 (2017).
64. C. S. C. Tan-Lim, N. A. R. Esteban-Ipac, J. B. V. Mantaring III, E. Chan Shih Yen, M. S. T. Recto, O. T. Sison, M. M. Alejandria, Comparative effectiveness of probiotic strains for the treatment of pediatric atopic dermatitis: A systematic review and network meta-analysis. *Pediatr. Allergy Immunol.* **32**, 124–136 (2021).
65. B. M. Ray, Performance auditing of an in vitro air pollution exposure system. *Toxicology* **10**, 615–624 (1998).
66. K. Urban, S. Chu, R. L. Giesey, S. Mehrmal, P. Uppal, N. Nedley, G. R. Delost, The global, regional, and national burden of atopic dermatitis in 195 countries and territories: An ecological study from the Global Burden of Disease Study 2017. *JAAD Int.* **2**, 12–18 (2021).
67. Y. Guo, P. Li, J. Tang, X. Han, X. Zou, G. Xu, Z. Xu, F. Wei, Q. Liu, M. Wang, F. Xiao, W. Zong, C. Shen, J. Li, J. Liu, Y. Luo, J. Chang, N. Sheng, C. Dong, D. Zhang, X. Dai, J. Zhou, C. Meng, H. Niu, X. Shi, X. Zhang, J. Xiang, H. Xu, Q. Ran, Y. Zhou, M. Li, H. Zhang, R. Cheng, X. Gao, H. Wang, H. Gu, L. Ma, Z. Yao, Prevalence of atopic dermatitis in chinese children aged 1-7 ys. *Sci. Rep.* **6**, 29751 (2016).
68. CDC, Toluene diisocyanate (TDI) and toluenediamine (TDA): Evidence of carcinogenicity (Current Intelligence Bulletin 53, CDC, 1989).
69. L. Fernandez, Toluene diisocyanate demand worldwide from 2011 to 2020 with a forecast for 2022. *Statista* (2021).
70. L. Fernandez, Methylene diphenyl diisocyanate production in the United States from 1990 to 2019. *Statista* (2021).
71. Markit, Isocyanates (Process Economics Program Report 1B, 1973).
72. MerchantResearch, Toluene diisocyanate (TDI): 2021 World market outlook up to 2030 (with COVID-19 impact estimation). *Research and Markets*, (2021).
73. W. Yen, How long and how far do adults travel and will adults travel for primary care? (Washington State Health Services Research, 2013).
74. J. Friedman, T. Hastie, R. Tibshirani, Regularization paths for generalized linear models via coordinate descent. *J. Stat. Softw.* **33**, 1–22 (2010).
75. M. N. Wright, A. Ziegler, ranger: A fast implementation of random forests for high dimensional data in C++ and R. *J. Stat. Softw.* **77**, 1–17 (2017).
76. B. M. Greenwell, pdp: An R package for constructing partial dependence plots. *R J.* **9**, 421–436 (2017).

Acknowledgments

Funding: This work was supported by the Intramural Research Program of the National Institute of Allergy and Infectious Diseases (NIAID) and the National Institutes of Health (NIH) and the NIH Medical Research Scholars Program. **Author contributions:** Conceptualization: J.Z. and I.A.M. Methodology: J.Z., P.P.C., J.S., M.Y., B.N.D., M.E.A., P.G., J.M., A.J.G., Y.L., L.F.E., E.L.S., and I.A.M. Investigation: J.Z., P.P.C., M.Y., P.G., A.J.G., Y.L., L.F.E., E.L.S., A.A.S., and I.A.M. Visualization: J.Z., P.P.C., and I.A.M. Supervision: I.A.M. Writing—original draft: J.Z. and I.A.M. Writing—review and editing: J.Z., P.P.C., J.S., M.Y., B.N.D., M.E.A., P.G., J.M., A.J.G., Y.L., A.A.S., L.F.E., and E.L.S. **Competing interests:** E.L.S. reports personal fees from AbbVie, Amgen, Arena Pharmaceuticals, Aslan Pharma, Boston Consulting Group, Collective Acumen LLC (CA), Dermira, Eli Lilly, Evidera, ExcerptaMedica, Forte Bio RX, Galderma, GlaxoSmithKline, Incyte, Janssen, Kyowa Kirin Pharmaceutical Development, Leo Pharm, Medscape LLC, Merck, Pfizer, Physicians World LLC, Regeneron, Roivant, Sanofi-Genzyme, Trevi therapeutics, Valeant, and WebMD. E.L.S. also reports grants (or principal investigator role) from AbbVie, Amgen, Arcutis, Aslan, CorEvitas, Dermavant, Dermira, Eli Lilly, Incyte, Kymab, Kyowa Hakko Kirin, Leo Pharmaceuticals, Pfizer, Regeneron, Sanofi, and TARGET-DERM. These potential conflicts of interest have been reviewed and managed by OHSU. L.F.E. reports grants and fees for participation as a consultant and/or investigator from AbbVie, Almira Il, Aslan, Dermavant, Dermira, Eli Lilly and Company, Forte Biosciences, Galderma, Incyte, LEO Pharma, Novartis, Pfizer, Regeneron, and Sanofi Genzyme, and honoraria and fees from Asana and Glenmark for data safety monitoring board services. All other authors have no competing interests. **Data and materials availability:** All data needed to evaluate the conclusions in the paper are present in the paper and/or the Supplementary Materials.

Submitted 14 September 2022
Accepted 5 December 2022
Published 6 January 2023
10.1126/sciadv.ade8898